HIGH POWER TRAVATRON INVESTIGATION

J. M. Proud, Jr., et al

IKOR, Incorporated

Prepared for:

Rome Air Development Center

August 1973

UNCLASSIFIED

SECURITY CLASSIFICATION OF THIS PAGE (When Data Entered)

REPORT DOCUMENTATION PAGE		READ INSTRUCTIONS BEFORE COMPLETING FORM
1 REPORT NUMBER RADC-TR-73-227	2 GOVT ACCESSION NO.	3. RECIPIENT'S CATALOG NUMBER
4 TITLE (and Subtitle) HIGH POWER TRAVATRON INVESTIGATION		5. TYPE OF REPORT & PERIOD COVERED Final Report 6 PERFORMING ORG. REPORT NUMBER None
7 AUTHOR(s) J. M. Proud, Jr. W. H. McNeill		8 CONTRACT OR GRANT NUMBER(s) F30602-72-C-0068
9 PERFORMING ORGANIZATION NAME AND ADDRESS IKOR, Incorporated Second Avenue Burlington, Massachusetts 01803		10 PROGRAM ELEMENT, PROJECT, TASK AREA & WORK UNIT NUMBERS 55730641
11 CONTROLLING OFFICE NAME AND ADDRESS Rome Air Development Center (OCTP) Griffiss Air Force Base, New York 13441		12 REPORT DATE August 1973 13. NUMBER OF PAGES ~~76~~ 84
14 MONITORING AGENCY NAME & ADDRESS(if different from Controlling Office) Same		15 SECURITY CLASS. (of this report) UNCLASSIFIED 15a. DECLASSIFICATION/DOWNGRADING SCHEDULE N/A

16 DISTRIBUTION STATEMENT (of this Report)

Approved for public release; distribution unlimited.

17 DISTRIBUTION STATEMENT (of the abstract entered in Block 20, if different from Report)

Same

18. SUPPLEMENTARY NOTES

None

19. KEY WORDS (Continue on reverse side if necessary and identify by block number)

Nanosecond Modulator
RF Generation
High Voltage Techniques

20 ABSTRACT (Continue on reverse side if necessary and identify by block number)

A program has been conducted to investigate techniques associated with enhancing the peak power generating capabilities of the Travatron. Analyses aimed at optimizing power-to-size ratios of the device and determination of operating limits are reported. Various techniques for generation of high voltage pulses suitable for driving the Travatron are analyzed and tested. A breadboard model Travatron generating over 10 MW peak power in 10 ns pulses at 1.3 GHz is also described.

DD FORM 1 JAN 73 1473 EDITION OF 1 NOV 65 IS OBSOLETE

UNCLASSIFIED

SECURITY CLASSIFICATION OF THIS PAGE (When Data Entered)

Nanosecond Modulator
RF Generation
High Voltage Techniques

FOREWORD

This Final Report was prepared by IKOR, Incorporated, Second Avenue, Burlington, Massachusetts, under contract F30602-72-C-0068, Job Order Number 55730641, for Rome Air Development Center, Griffiss Air Force Base, New York. It describes research accomplished between 21 October 1971 and 31 December 1972. Mr. Frank E. Welker (OCTP) was the RADC Project Engineer.

This report has been reviewed by the RADC Information Office (OI) and is releasable to the National Technical Information Service (NTIS).

This technical report has been reviewed and is approved.

APPROVED: Frank E Welker
FRANK E. WELKER
Project Engineer

APPROVED: William T. Pope
WILLIAM T. POPE
Assistant Chief
Surveillance & Control Div

FOR THE COMMANDER: Carlo P Crocetti
CARLO P. CROCETTI
Chief, Plans Office

ABSTRACT

A program has been conducted to investigate techniques associated with enhancing the peak power generating capabilities of the Travatron. Analyses aimed at optimizing power-to-size ratios of the device and determination of operating limits are reported. Various techniques for generation of high voltage pulses suitable for driving the Travatron are analyzed and tested. A breadboard model Travatron generating over 10 MW peak power in 10 ns pulses at 1.3 GHz is also described.

EVALUATION

The objective of this effort was to investigate techniques aimed at determining the maximum peak power and pulse length capability of the travatron type RF generators. The devices are for use in lightweight high peak power transmitter experiments in support of TPO 18.

The travatron is a RF generation device for short very high peak power radio frequency pulses. It uses a series of spark gaps separated by short segments of transmission line to chop a video pulse into RF cycles. The specific areas of investigation were the spark gaps, the optimum impedance level for the line segments and video voltage generating schemes for charging the video pulse forming line. Early in the effort it was predicted that low impedance lines (under 20 Ω) were best for high power operation. However, when the spark gap characteristics were included in the calculations lines of much higher impedance (over 100 Ω) were necessary for operation at high power above a few hundred megacycles. Several practical voltage multiplication schemes were breadboarded and their limitations determined. A breadboard model was fabricated that confirmed the calculated effects of spark gaps, line impedance, etc.

Frank E Welker

FRANK E. WELKER
Proj Engr/OCTP

TABLE OF CONTENTS

LIST OF ILLUSTRATIONS

SECTION I

INTRODUCTION

The Travatron is a novel transmitting device[1] for the generation of short, high power radio frequency pulses. Operating on a principle whereby input video pulse energy is efficiently converted directly to rf energy, the Travatron can overcome many of the obstacles of complexity and high costs as well as weight and size penalties associated with competing short pulse techniques.

Various models of the Travatron have been fabricated and used at VHF and L-Band. A reliable L-Band device generating three megawatts of peak power has been used extensively at RADC[2]. The concentration of the development efforts to date have centered on the realization of the dc-rf conversion mechanism. As a part of this prior work, certain peripheral developments have also been accomplished as related to high peak power handling in signal separators, resistive terminations and other hardware elements specifically tied to the generation, extraction and handling of the rf signal.

The objectives of the program reported here have been two-fold. The primary objective was to investigate means for raising the peak power capability of the Travatron. Secondly, methods for meeting the unique requirements of the video generator portion of the Travatron transmitter were to be explored.

The approach toward increased power capability was broadened in the program to include optimization analysis of power-to-size ratio, the use of high dielectric constant materials and analysis of peak power limits. Overall, order of magnitude improvement in peak power as well as power-to-size ratio has been achieved.

Pulse power investigations have included the first successful use of a fast Blumlein PFN as a video pulse input device for the Travatron. In addition, a unique high voltage pulser employing the piezoelectric effect

has been demonstrated as well as several more conventional pulsers.

Travatron design analysis is presented in Section II. Section III deals with the various techniques analyzed and breadboarded in the investigation of video pulse generator candidates. An integrated Blumlein-Travatron breadboard is described in Section IV which demonstrates many of the design concepts and analyses developed in this program. Conclusions and recommended are found in Section V.

SECTION II

TRAVATRON DESIGN ANALYSES

The operating principles and theory of the Travatron are presented in this Section. The utilization of the dielectric material in the coaxial Travatron is then examined to show that an optimum impedance exists for any particular dielectric which maximizes the power to volume ratio. Switch function is then examined to show that high power design may require high impedance values. The analyses are then applied to the design of Travatrons operating at 1, 10 and 100 MW.

1. BASIC OPERATING PRINCIPLES AND PROPERTIES

The Travatron is a traveling wave device employing spark gap switches which provides a means for efficient and direct conversion of dc to rf energy in short pulse bursts. The process is one in which an input rectangular voltage pulse, derived from a video pulse generator or "modulator", is chopped by means of a sequence of spark switch closures to produce an rf burst. The conversion mechanism can be described briefly with reference to Figure 1 which illustrates the basic traveling wave structure of the Travatron (usually coaxial). The structure is composed of a sequence of quarter wave transmission line segments each separated by a spark switch. As the input rectangular pulse propagates through the structure it encounters the switches in sequence. The switches, designed to close in one-half rf period, each reflect one-half cycle of rf. The result is the reflected, chopped wave as indicated. The rf coupler passes the desired rf component, (about 40% of the pulse energy) and reflects the remainder of the spectrum back into the structure where it is absorbed in the termination.

Figure 2 is an idealized energy conversion diagram illustrating the function of the Travatron and the energy partition into the components of the generated pulse. The initial video pulse, propagating in a transmission line of characteristic impedance Z, possesses energy E_o given by:

$$E_o = V^2 \tau/Z \qquad (1)$$

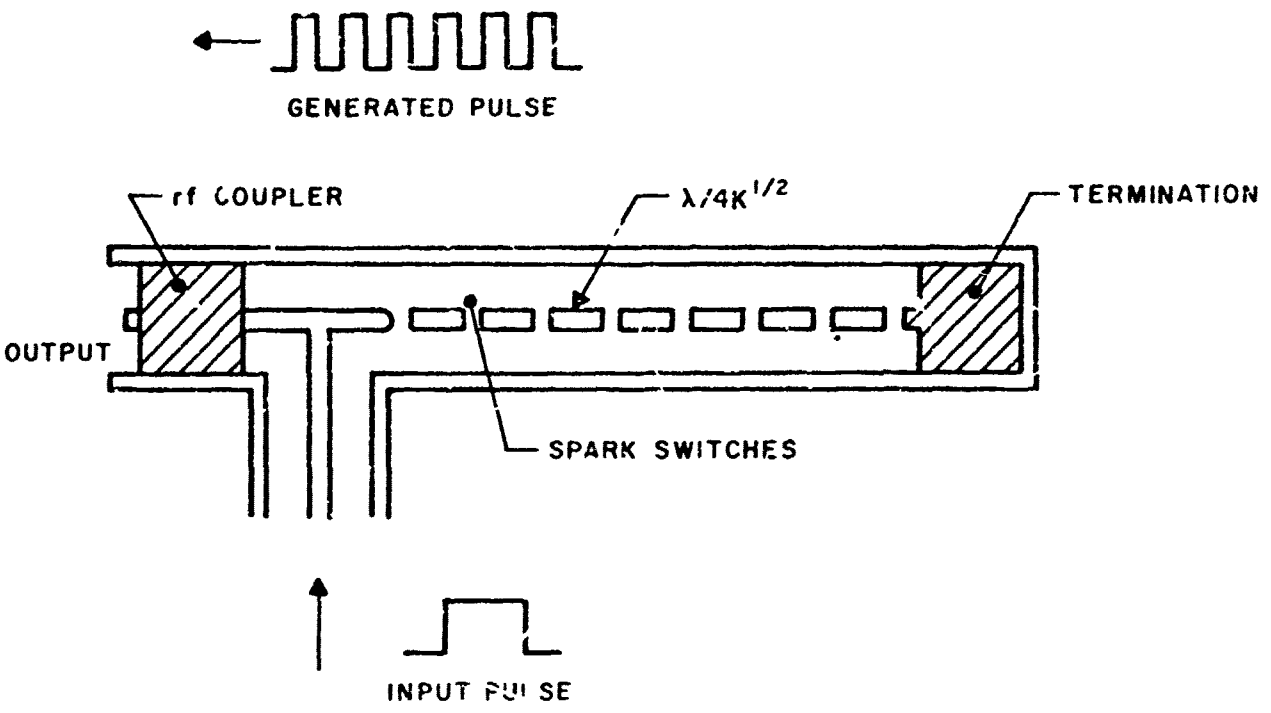

FIGURE 1
TRAVATRON STRUCTURE

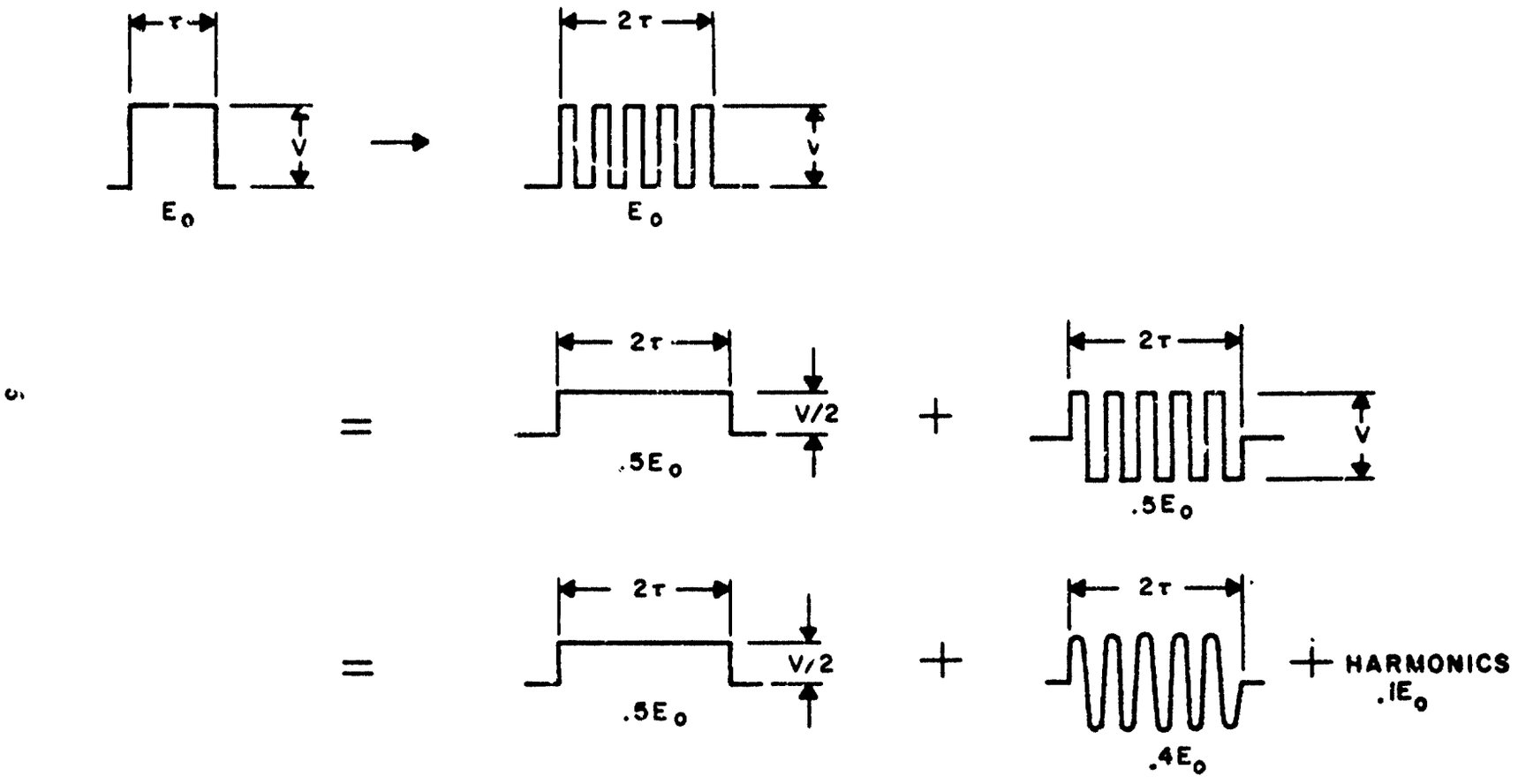

FIGURE 2

ENERGY CONVERSION DIAGRAM FOR TRAVATRON

where V is the traveling wave pulse height and τ is the pulse length. By the process described above, the sequential switching of the Travatron chops and redistributes this energy into a pulse of the same height and twice the length as illustrated.

By superposition principles, the pulse illustrated on the first line in Figure 2 may be resolved as shown into a dc pulse and a square wave having no dc component. Each pulse has energy:

$$(V/2)^2 \cdot 2\tau/Z = E_o/2 \qquad (2)$$

The rf square wave may be further resolved as illustrated into a pulsed sine wave plus the higher frequency harmonics associated with the square wave (the odd harmonics). Approximately 80% of the square wave energy is contained in the fundamental sine wave. Therefore, the efficiency is 40% and the peak power P is given by

$$P = 0.4\, E_o/2\tau = 0.2\, V^2/Z \qquad (3)$$

The conversion process is further illustrated in the frequency domain in Figure 3 showing the results of Fourier analysis for a Travatron pulse containing 10 cycles of rf. The spectrum indicated by the dashed line is that of the initial modulator pulse, while the solid line is a plot of the spectrum for the chopped pulse burst. The large low frequency component results from the dc off-set of the wave train. This characteristic is readily exploited in that band-pass requirements for extracting rf energy from the device may be met effectively with simple high-pass filters. Further, the energy not extracted is of relatively low frequency and may be easily absorbed and dissipated.

The general relations for rf center frequency f_o and bandwidth Δf are

$$f_o = N/2\tau \quad \text{and} \quad \Delta f = 2f_o/N \qquad (4)$$

where N is the number of rf cycles.

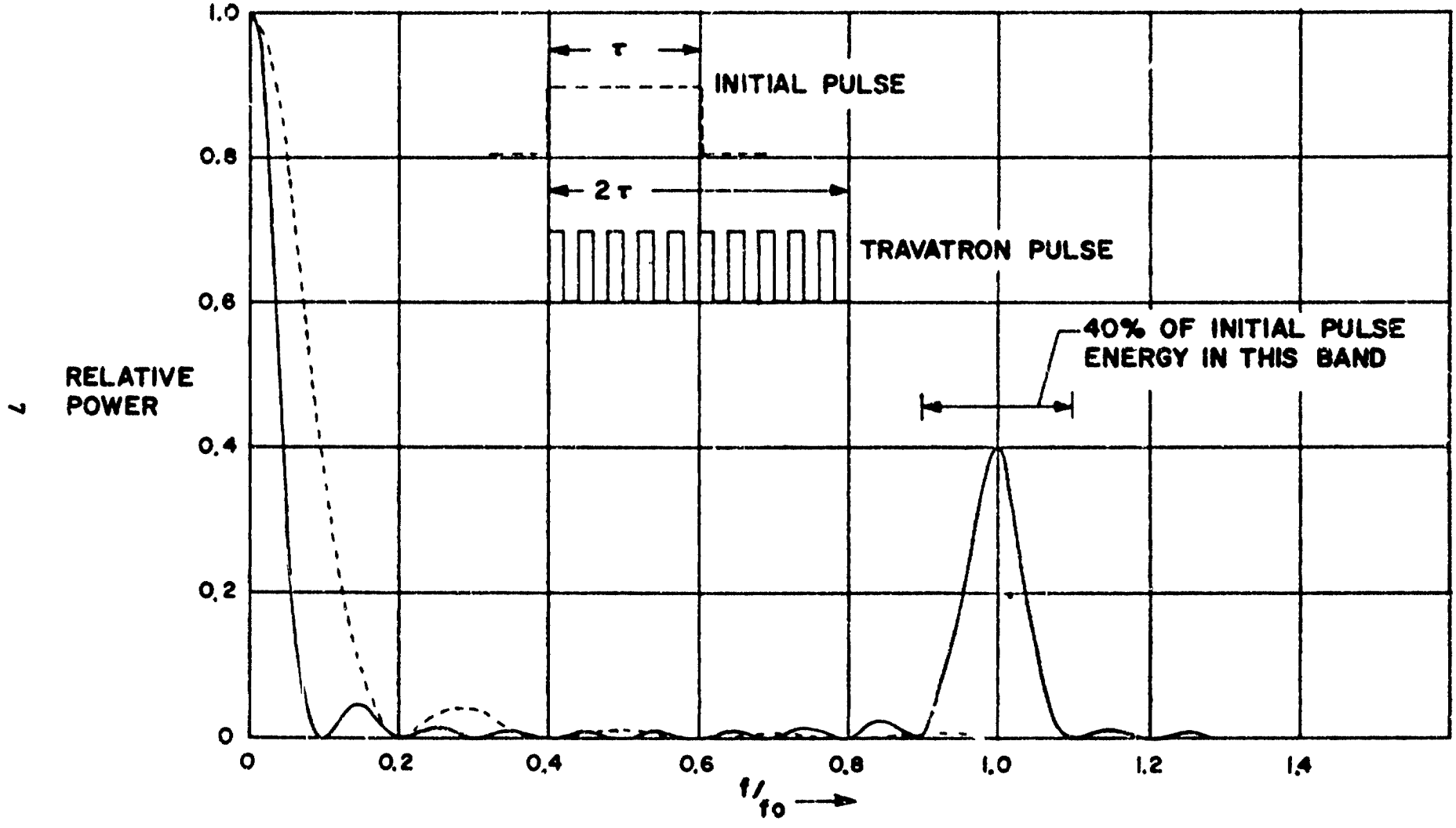

FIGURE 3

POWER SPECTRUM CONVERSION

The Travatron possesses several unique characteristics which make it an attractive source of high peak power, short duration pulses. Inasmuch as the Travatron employes spark switches whose closures are governed by high over-voltage field strengths, the peak voltages and, therefore, the peak powers generated are generally large. The device is then inherently a source for peak power pulses in the megawatt range and above. Moreover, it appears that direct extension to the gigawatt range should be feasible.

Initially, the motivation for developing the Travatron was to attain a short pulse source for radar application wherein the Travatron could eliminate the undesired complexity of pulse compression systems in many applications. The simplicity and high peak power to size ratios obtain when pulse lengths are in the nanosecond range (depending on rf frequency). Experience has shown that the Travatron exhibits its greatest advantage over other pulse generator techniques when the output pulse contains fewer than about twenty rf cycles.

An important characteristic of the Travatron for many applications is its "first-pulse capability". Thus, through the use of cold cathode spark switches, the device requires no warm-up. As a corollary there is no stand-by power consumed. It is well suited, therefore, to application where zero power is consumed until an instant turn-on is required. Of course, the absence of filament power, magnetic fields, etc. are equally important in obviating complexity in the transmitter design.

Ideally, the output spectrum of the Travatron is that of a wideband square wave. With attention to switch jitter and harmonic suppression, the output can be made to conform to a sine wave pulse with reasonable spectral purity. On the other hand, if a noisy, skewed or tailored spectrum is desired, this can be easily accommodated. In fact, the pulse output can be designed to possess a swept frequency. This flexibility stems from the fact that each rf cycle is individually formed by one transmission line section and one spark switch and there are no narrow band or resonant structures in the basic Travatron.

2. OPTIMUM STRESS CONFIGURATION

Models of the Travatron which have been designed and constructed prior to this program have exhibited a high ratio of peak power to physical size, although no attempt has been made to extend or optimize the design toward minimum size or weight. The following analysis was undertaken with the goal of determining an optimum stress configuration for the coaxial Travatron. The results indicate a utilization of the dielectric material which maximizes the power-to-volume (of dielectric) ratio. It also prescribes an impedance value for any particular dielectric material.

Ignoring other factors, the analysis suggests the use of dielectric material having a high dielectric constant and relatively low values of impedance. This, in turn, prescribes relatively low voltage needs for a given peak power level. These results must be applied carefully, however, as a subsequent analysis based on spark gap switching phenomena shows that absolute peak power limits are directly proportional to impedance. Thus, for situations where the upper bounds of peak power are desired, a higher impedance value must be chosen than would be prescribed by the optimum stress analysis.

From Equation (3) above, the peak power in the pulsed sine wave generated by the Travatron is given, ideally, by:

$$P = 5 \times 10^{-2} V_o^2 / Z \tag{5}$$

where Z is the characteristic impedance and V_o is the open circuit voltage appearing at each switch in the Travatron. The impedance in a coaxial device is:

$$Z = 1/2 \, \pi \, (\mu/\epsilon)^{1/2} \ln R = 60 \, K^{-1/2} \ln R \tag{6}$$

where R is the ratio of outer to inner conductor radii, b and a respectively. The radial voltage stress is:

$$E_r = V_o / r \ln R \tag{7}$$

with a maximum at r = a

$$E_a = V_o/a \ln R \tag{8}$$

The Travatron peak power can then be written in the form:

$$P = 8.3 \times 10^{-4} K^{1/2} E_a^2 b^2 \ln R/R^2 \tag{9}$$

Now, for a fixed dielectric constant, a fixed outer conductor radius b, and a fixed maximum stress $E_a = S$, the power relation (9) has a maximum at $\ln R = 1/2$. This yields an "optimum" impedance from equation (6) given by:

$$Z = 30 K^{-1/2} \tag{10}$$

where K is the relative dielectric constant. The peak power is then:

$$P = 1.54 \times 10^{-4} b^2 S^2 (K)^{1/2} \tag{11}$$

and the open circuit voltage from (8) is given by:

$$V_c = 0.30 bS \tag{12}$$

Equations (10), (11), and (12) then define the impedance, peak power and open circuit voltage in terms of the dielectric material properties K and S and the physical dimension, outer radius b.

The use of high K materials is seen to reduce device diameter, operating voltage and impedance. In addition, since the physical length of the Travatron exhibits a $K^{-1/2}$ dependence, this dimension is also reduced. In fact, the power-to-volume (of dielectric) ratio is proportional to KS^2 as might be anticipated from energy density considerations.

Generally, to minimize volume, at least the dielectric volume, one chooses a dielectric having a KS^2 product as large as possible. The relationship (10) then provides the impedance which optimizes the use of that particular dielectric and the other parameters follow from (11) and (12). If an impedance is desired which is not the optimum for a particular voltage of K, the more general relations (6), (8) and (9) must be used.

3. SWITCH CONSIDERATIONS

The function of the Travatron depends critically on the function of the switches used in the traveling wave structure. Ideally, such switches are called upon to remain in the open state for a time equal to one half period of the rf frequency and, subsequently, to close abruptly in a time much less than the rf period. The duration of the open state is generally governed by the statistical lag time[3] plus the formative time[4]. In addition, the closure rise time may also be affected in an important way by inductance.

The objectives of this program were, in part, to establish design guidelines for multi-megawatt or higher peak power capability at frequencies near 1 GHz. Concern is, therefore, with open state switch duration of about one-half nanosecond followed by tenth-nanosecond closure time. It is of interest to consider the possible impact of spark switch performance on these high power design parameters.

The statistical lag in an over-volted, non-illuminated spark gap is governed largely by the field emission of electrons from the cathode. Direct measurements of the statistical component of lag[3] show, typically, a lag of the order of 10^{-9} sec for fields near 10^5 volts/cm failing to less than 10^{-10} sec at fields near 10^6 volts/cm. Prior Travatron experience has involved field strengths over this range with the lower field values associated with low power VHF performance and higher fields associated with high power L-Band devices. In the investigation of statistical lag versus applied field for spark gap conditions similar to those found in the Travatron, some success (see Figure A-1 of Reference 3) was found in fitting the data with a Fowler-Nordheim dependence:

$$t_s = 7000/E^2 \exp(870/E) \qquad (13)$$

where t_s is the statistical lag in nanoseconds and E is the applied field in kilovolts/cm.

The formative time is a measure of the time required for free electrons to form an electron avalanche following a sudden voltage stress. Operationally, it is

measured[4] as the time required for a detectable reduction in impedance of an open spark having initiating electrons present subjected to a voltage step. In all prior experience with the Travatron, the conditions of applied field and gas pressure have been such that the formative time is very small compared to the observed closure times of the Travatron switches. In fact, with the high field strengths which usually apply, particularly at high power, formative time accounts for only a small fraction of the closure lag.

At the onset of breakdown in a fast closing spark switch, many processes take place which have strong time dependencies. Macroscopically, these manifest themselves in the complex impedance of the switch. While oversimplifying the situation, it is instructive to consider this impedance to be primarily inductive. Then, the rise time of the transmission line switch will be given approximately by:

$$t_r = 2L/Z \tag{14}$$

A consideration of this model of the Travatron switch suggests that a peak power limit exists. Thus, as the gap space is increased to maintain a particular statistical lag time for increasing applied voltage, the inductance will also increase to the point where it may dominate the switch closure time and prevent the proper function of the Travatron. To quantify this limit further, an approximate analysis has been carried out based on the two relationships (13) and (14).

For proper Travatron function according to this model the statistical lag time must be equal to one-half period of rf. Thus,

$$t_s = 1/2\, f_o \tag{15}$$

At f_o = 1 GHz, the required field strength at the cathode surface is given by the solution of

$$7000/E^2 \exp(870/E) = 0.5 \text{ ns} \tag{16}$$

which yields, approximately, E = 375 KV/cm. Now, the open circuit voltage at each Travatron switch will be V_o or twice the traveling wave height V. For uniform field conditions, the applied field is then simply determined by

V_o/d where d is the gap space. Using Equation (5), d can then be written in terms of the peak power and impedance

$$d = .012\ P^{1/2}\ Z^{1/2}\ \text{cm} \tag{17}$$

where P is expressed in megawatts. Values of d given by this expression are not substantially different from those determined empirically in previously designed Travatrons, thereby lending support to the model used for the estimate.

The switch rise time must be substantially less than one quarter cycle of rf. Thus, from Equation (14) the following inequality must hold

$$2\ L/Z < (4\ f_o)^{-1} \tag{18}$$

Then, for f_o = 1 GHz,

$$L < .125\ Z\ \text{nh} \tag{19}$$

To estimate the inductance, a very simple model of the spark gap switch is chosen consisting of a centered filamentary spark channel of constant radius a. The outer conductor of the coaxial geometry has radius b. The inductance of the spark channel is then given by

$$L = \mu_o/2\pi \cdot \ln b/a \cdot d \tag{20}$$

The spark channel diameter is not well known. However, it is not unreasonable to choose a value of b/a range of 10^2 to 10^3 for typical Travatron geometry. Moreover, the analysis is quite insensitive to the ratio in view of the logarithmic dependence. For purposes of the present estimate, the natural log has been sent equal to 5, yielding

$$L = 10\ d\ \text{nh} \tag{21}$$

when d is expressed in cm. Substitution in the inequality (19) yields

$$d < .0125\ Z\ \text{cm} \tag{22}$$

Combining (22) and (17) gives

$$.012\ P^{1/2}\ Z^{1/2} < .0125\ Z$$

or

$$P < 1.1\ Z \qquad (23)$$

The relationship (23) may be interpreted as a statement of the maximum power level obtainable at 1 GHz for a particular value of impedance. Similar estimates of the peak power limit at other frequencies are summarized in Table I in terms of the ratio P/Z. Figure 4 illustrates the same results graphically where the peak power limit is plotted as a function of frequency for various impedance values.

TABLE I

Travatron Peak Power Limits at Various Frequencies (simplest structure)

f_o(GHz)	P/Z (MW/ohm)
0.1	42
0.5	3.2
1.0	1.1
2.0	.39
5.0	.098

The general result is that a very high peak power design requires a higher rather than lower impedance Travatron. In establishing the design parameters for any particular Travatron peak power objective, the limit relationship (23) should supplement and supersede the design criteria developed above which were based upon optimum utilization of the dielectric material.

The above analysis is incomplete in several respects since it does not account for such factors as rise time of the incident pulse, spark channel resistance or gap capacitance. However, it is interesting to note its application to the present program. The Travatron model breadboarded in this

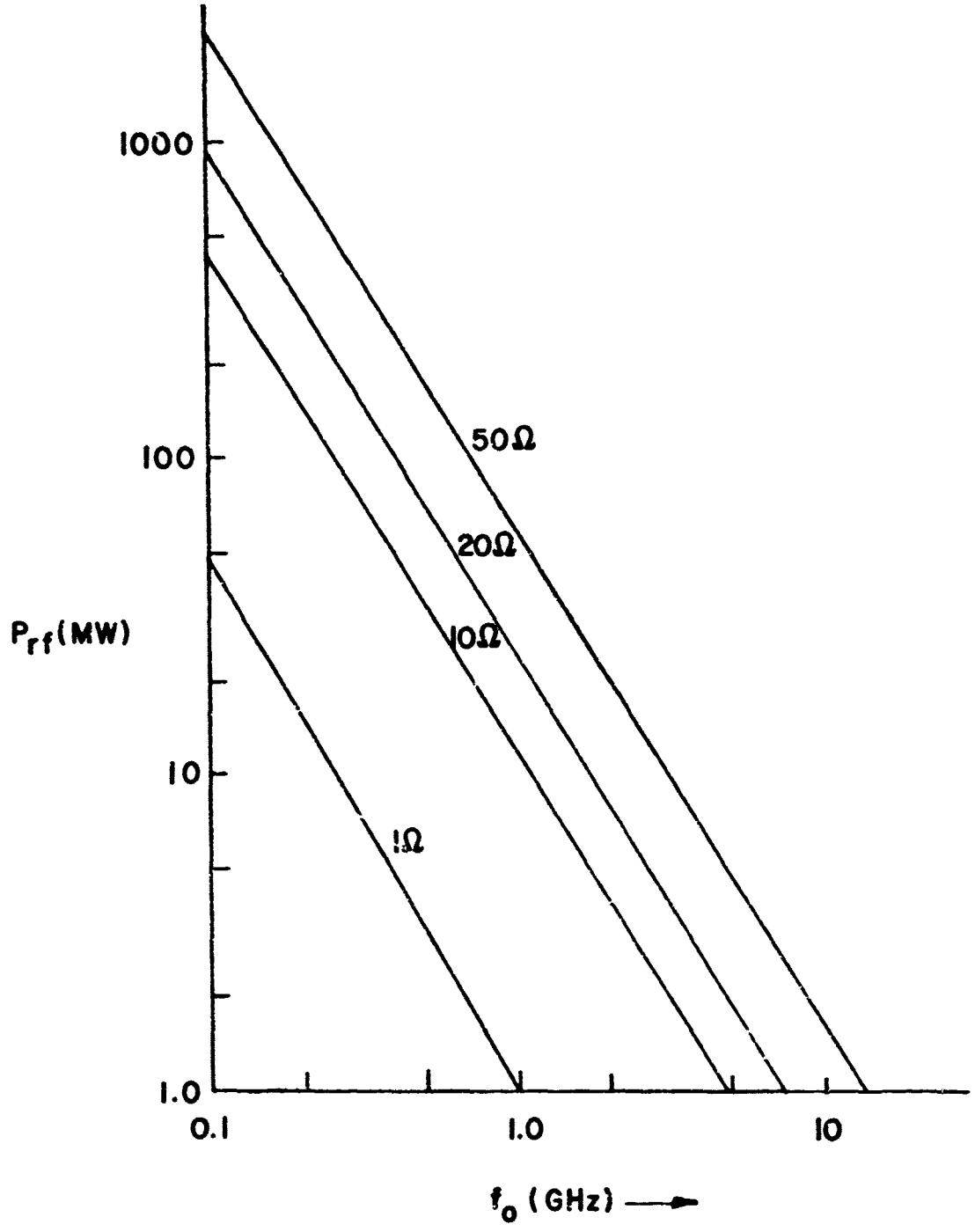

FIGURE 4

ESTIMATED PEAK POWER LIMIT vs FREQUENCY FOR SINGLY SWITCHED TRAVATRON

program was designed before this analysis was conducted and, therefore, followed the design procedure suggested by the optimum stress configuration. Specifically, an impedance value of approximately 17 ohms was selected and, depending upon the input pulse heights, peak power levels in the 10 to 100 MW range were expected to result at the design frequency of 1.3 GHz. This expectation did not materialize, however, and the peak power limit for the device constructed was very close to 10 MW. Reference to Figure 4 suggests that this limit, encountered experimentally, was due to the switch phenomena analyzed here. Moreover, to achieve 100 MW would have required a device impedance of approximately 130 ohms.

The above limits apply to a simple coaxial Travatron. Other geometries, for example those involving parallel traveling wave structures, could offer solutions to peak power extensions substantially above the limits cited for the singly switched case in Table I and Figure 4.

4. DESIGN APPLICATION

The application of the above analyses can best be illustrated by applying the results to specific objectives. Three peak power levels are considered in the following at 1 MW, 10 MW and 100 MW and an rf frequency of 1.0 GHz is assumed. It is seen that each peak power level introduces somewhat different application of the analysis.

An important factor affecting the design approach considered in this program is the availability of material covering a wide span of dielectric constant. Such material is available* with values of K ranging from 3 to 23 in machinable stock suitable for use in the Travatron permitting considerable freedom in choosing a dielectric. The material exhibits good high voltage properties as well as low microwave dissipation.

---

*Manufactured by Emerson & Cuming, Incorporated, Canton, Massachusetts, under trade names of Stycast HiK and Stycast HiHiK.

a. 1 MW Design

From the inequality (23) the impedance for a 1 MW Travatron at 1 GHz should be about one ohm or larger. Choosing a dielectric constant having a value K = 23, the impedance for optimum stress utilization is 6.25 ohms from (10).

The maximum electric stress for this material is estimated by the manufacturer to exceed 200 volts/mil. There is evidence to suggest that higher values such as 500 volts/mil are reasonable especially where the stress is applied for durations less than about 10 nanoseconds as is the case in the Travatron structure of concern here. Therefore, in applying equation (11) the larger value, S = 500 volts/mil, has been used yielding: b = .074 in., a = .045 in. and V_o = 11 KV. For a 10 ns pulse output the physical length of such a Travatron would be 6.25 in. and the volume of the traveling wave structure would be only 0.11 $in.^3$. At this power level, considerably freedom exists to choose dielectric constant values and impedance. Lesser values of K will of course result in larger physical size but the designs will be equally workable. As seen below, this latter factor is not true for extended power design.

b. 10 MW

At 10 MW the inequality (23) requires that the impedance be larger than about 10 ohms. In using (10) it is seen that a K of 23 will not permit optimum use of the dielectric at this impedance level, although a reasonable design can be achieved with K = 23. The only value of K which will satisfy optimum conditions at 10 ohms is K = 9. The design parameters then become: b = .30 in., a = .21, V_o = 45 KV, length = 10 in. and traveling wave structure = 2.8 $in.^3$.

c. 100 MW Design

At 100 MW the inequality (23) requires an impedance of about 100 ohms or greater. Reference to (10) reveals that optimum utilization of dielectric cannot be achieved since K cannot be less than unity. Furthermore,

the high K materials give rise to unacceptable design parameters at this power level generally because the departure from the optimum dielectric use is so great. For example, if value of K = 23 is selected, the dimension b becomes 337 in! Even when K = 2.3 (as is typical of commonly used plastic materials) the radius b is 7.2 in. and a is 0.6 in. The situation is one in which b-a is comparable to a wavelength in the material, a condition which invites the propagation of other than the lowest TEM mode required for proper Travatron function. The suggested design approach is then to choose a low value of K = 1 such as might be attained with a pressurized gas dielectric.

The open circuit voltage V_o for a 100 MW Travatron designed for 100 ohms impedance is 450 KV. The maximum stress is highly variable in a gas as it depends upon the gas pressure as well as the gas species. It is desirable to keep E_a below a value supporting significant field emission, e.g. 20^ KV/cm or about 500 volts/mil. Moreover, this stress, while equal to that used for the solid dielectrics considered above, can readily be attained in gases such as dry air at pressures near 100 PSIG. Using this value of stress, a = .52 in. and b = 2.8 in. The length and volume of the structure are then 30 in. and 738 $in.^3$, respectively.

The design parameters for three Travatrons at 1, 10 and 100 MW having 10 ns pulse widths are tabulated in Table II for illustration. The parameters listed do not preclude other designs. However, as noted above, the flexibility of the design approach diminishes dramatically at higher power levels. The freedom of using high K values at lower peak power levels leads to very high ratios of power-to-volume which cannot be attained at higher powers.

TABLE II

Design Parameters for Three Travatrons

P(MW)	1.0	10	100
Z(ohms)	6.25	10	100
K	23	9	1
V_o(KV)	11	45	450
b(in)	.074	.28	2.8
a(in)	.045	.16	.52
l(in)	6.25	10	30
v(in^3)	.11	2.5	738

SECTION III

MODULATOR INVESTIGATION

1. GENERAL CONSIDERATIONS AND APPROACH

The Travatron possesses unique pulse input requirements which become progressively more difficult to attain as the output peak power is increased. In general, the modulator for the Travatron must deliver a fast, high voltage pulse having a height V with an output impedance matching the impedance of the Travatron structure. The width of the pulse should be one half of the width of the desired rf pulse, as may be seen with reference to Figures 2 and 3 above.

Typically, the modulator output pulses must be in the 20 to 200 KV range with an output impedance of 10 to 100 ohms to achieve the high power operation illustrated in Table II. The pulse width must be approximately 5 ns with a correspondingly short risetime.

In previous Travatron transmitters, the modulator pulse was attained by means of a coaxial line serving as a distributed parameter PFN. A high pressure spark switch served as a line-type modulator switch having sufficiently fast risetimes to enable the generation of reasonably rectangular, high voltage pulses of a few nanoseconds duration. The pulse forming line was charged resistively from a dc power source. While this modulator technique has served to provide repetitive pulses of the correct shape and amplitude, the method has several inherent shortcomings with respect to size, weight and efficiency. Furthermore, practical design considerations limit pulse amplitude due to difficulty in dc voltage handling at high potentials.

The investigation reported here approached the modulator design and evaluation as indicated in Figure 5. A complete Travatron transmitter is illustrated with several alternative modulator schemes. In each case, the modulator technique is a two-step process whereby a pulsed high voltage source impulse charges a pulse shaping circuit or PFN. The requirement for two steps seems to be quite basic because most (if not all) of the pulse

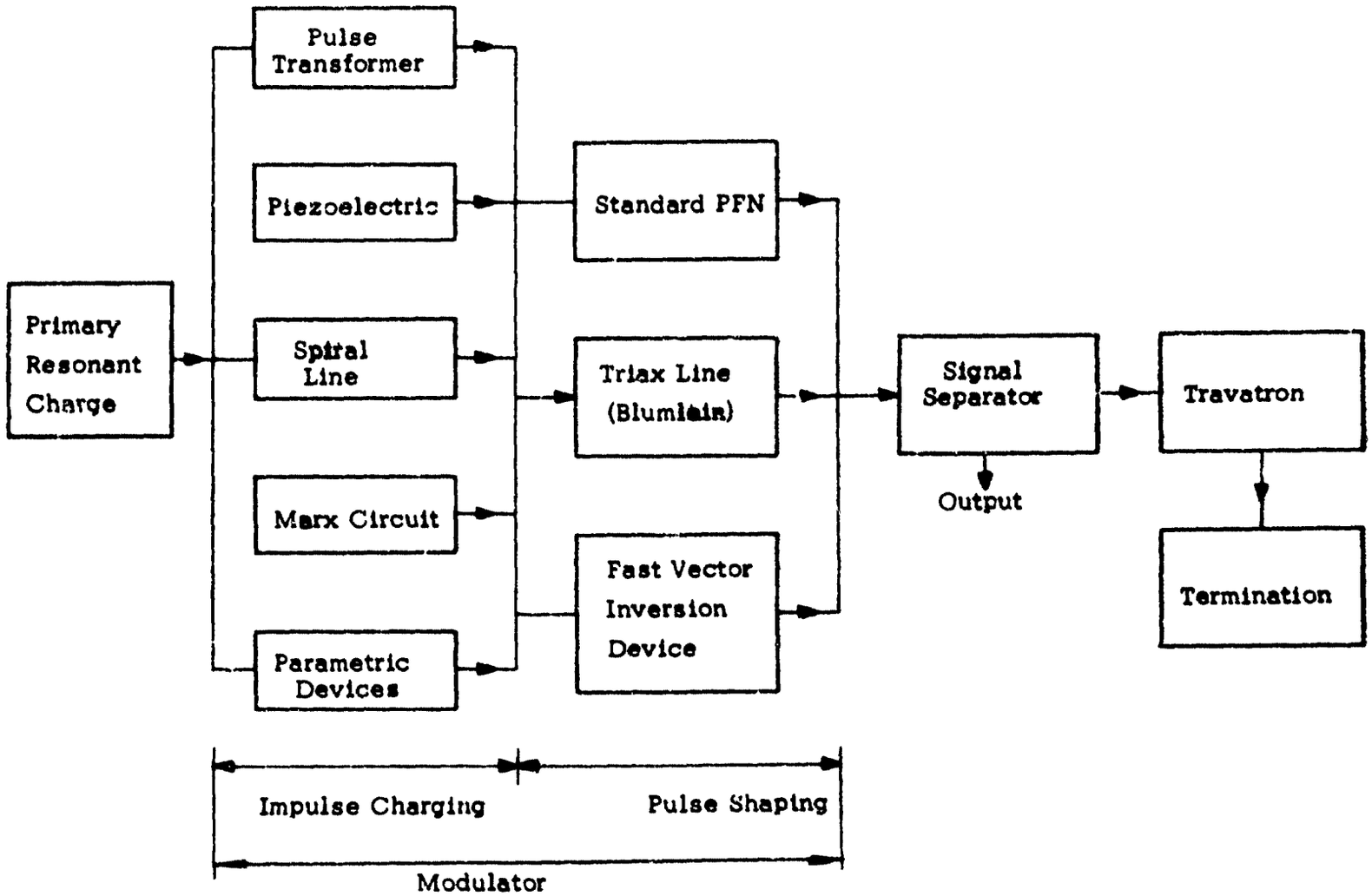

FIGURE 5

TRAVATRON SYSTEM APPROACHES

methods considered for high voltage generation are relatively slow compared to the nanosecond scale of interest. Although it would be highly attractive to generate the high voltage needed within the PFN structure, it does not appear possible with the exception of some form of piezoelectric generator.

Three pulse shaping schemes were considered in the program including a standard coaxial PFN, a triaxial Blumlein and other fast vector inversion devices such as stacked lines. Emphasis was placed on development of a suitable Blumlein since this device is capable of forming the required rectangular pulse with voltage doubling while it possesses some of the simplicity of the standard PFN. Thus, the Blumlein outperforms the standard PFN but avoids the complexity associated with most other vector inversion devices.

Several means were considered for the impulse charging role. Most straightforward is the technique using a pulse transformer. The breadboard model transmitter was designed to employ such a transformer. In addition, a piezoelectric generator was developed which used compressed gas as a prime energy supply. A spiral line generator was breadboarded to demonstrate that such a generator having suitable outputs could be constructed in a reasonably package. Finally, Marx circuits and parametric devices were considered on an analytical basis but were not breadboarded for evaluation in this program.

The design of the PFN and its associated fast closure switch(es) is generally eased if the charging voltage is applied rapidly. Dielectrics can be stressed substantially above their dc breakdown levels when the charging time is about 100 ns or less. Moreover, the overvolted switch can be designed with more freedom in this time domain and can therefore meet other constraints such as a highly confined geometry in the triaxial Blumlein. The source of high voltage designated as impulse charging devices do not naturally provide sufficiently fast risetime to meet the fast charging needs of the PFN. For example, high voltage pulse transformers are typically limited to risetimes in the microsecond domain while piezoelectric sources provide charge build-up at even slower rates as governed by the application of mechanical stresses. An efficient scheme using an intermediate transfer

capacitance followed by resonant charging of the PFN has been used extensively in the program to speed the energy transfer. The basic design theory is, therefore, reviewed in the next paragraph. Subsequently, the various high voltage pulse sources are described. Finally, the design and testing of the PFN portion of the modulator is reported.

2. RESONANT TRANSFER CIRCUIT

The basic resonant transfer circuit is shown in Figure 6. The transfer capacitance C_t is charged from the high voltage source and subsequently switched through the inductance L to charge the PFN, represented by the lumped capacitance C_p. If q_o is the initial charge on C_t, the charge q appearing on C_p is given by:

$$q = C/C_t \cdot q_o (1 - \cos \omega t) \tag{24}$$

where

$$C^{-1} = C_t^{-1} + C_p^{-1} \tag{25}$$

and

$$\omega = (LC)^{-1/2} \tag{26}$$

The expressions for current I, voltage V_t on C_t, voltage V_p on C_p, energy in C_t, energy in L and energy in C_p all follow in simple fashion. The most important situation is at a time corresponding to $\omega t = \pi$ when the maximum voltage occurs on C_p, the energy transfer is maximum and the current is zero. At this time, the voltage V_p and energy E_p relations are:

$$V_p = 2 V_o C_t (C_t + C_p)^{-1} \tag{27}$$

and

$$E_p = 2 V_o^2 C_t^2 C_p (C_t + C_p)^{-2} \tag{28}$$

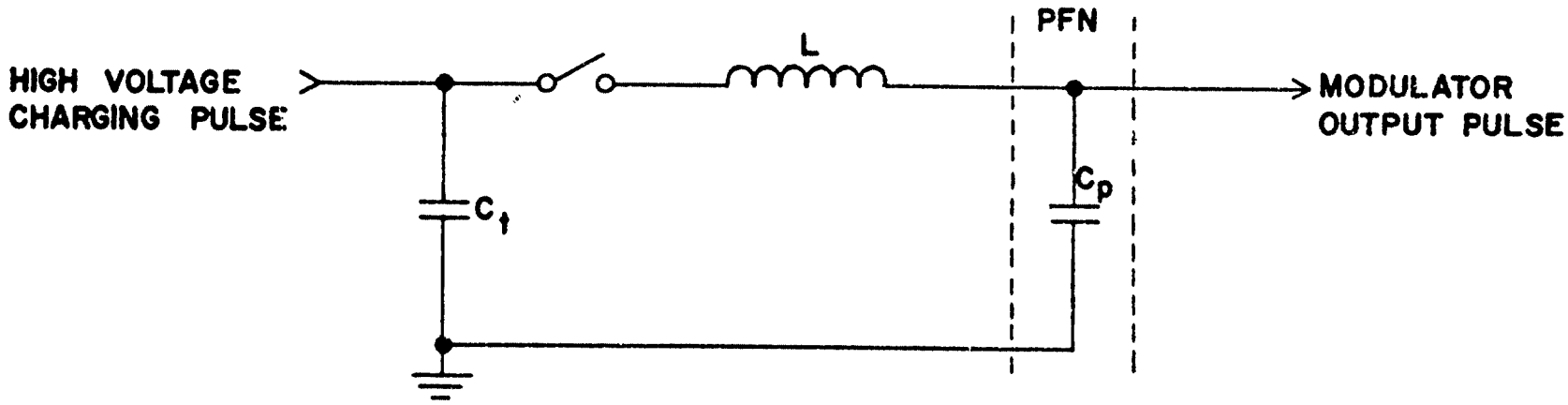

FIGURE 6

RESONANT TRANSFER CIRCUIT

Two cases are of particular interest. When $C_t >> C_p$, the maximum voltage on C_p is approximately $2V_o$. Thus, voltage doubling can occur, but the efficiency is small since this quantity approaches $4\ C_p/C_t$ when the above inequality applies.

In the second special case of interest, $C_t = C_p$. Under these conditions, the efficiency is 100% (except for any resistive losses) and the charge voltage on C_p has a maximum value of V_o. In practice, it is frequently desirable to form a compromise where C_t is chosen to be somewhat larger than C_p in order to achieve some voltage step-up at the expense of optimum efficiency.

3. PULSE TRANSFORMER CHARGING

a. Design Considerations

The most straightforward of the voltage pulse charging schemes considered in this program was the pulse transformer used with the above described resonant transfer circuit to develop a fast impulse charge within the PFN. In designing a specific transformer, the investigation focussed upon the two capacity discharge systems depicted in Figure 7.

In the step-charge scheme, low energy pulses are passed through the holding diode D to build up the potential on C_t in a step-wise fashion. The general design advantage of the method is that the energy handling capability of the primary circuit and transformer need be only a fraction of that placed on C_t. However, average power handling is independent of the number of steps used, while the repetition rate in the primary circuit is proportional to the number of steps used to charge C_t. Voltage levels in the primary circuit are modest and it is possible to use semi-conductor switches in the role of S_1. However, the peak voltage capability of the transformer must ultimately equal the charge voltage on C_t.

The single pulse charging scheme (Figure 7b) differs from the step-charge approach in that a holding diode is not required (although it may be useful) and the primary circuit is generally operated at a higher potential with the full pulse energy. A Travatron designed to deliver 10 to 100 MW

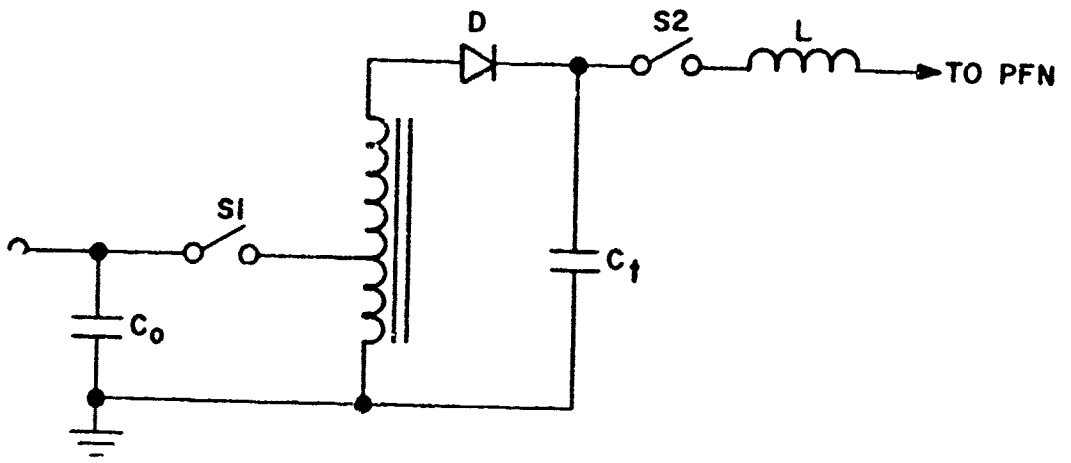

(a) STEP-CHARGING WITH AUTOTRANSFORMER

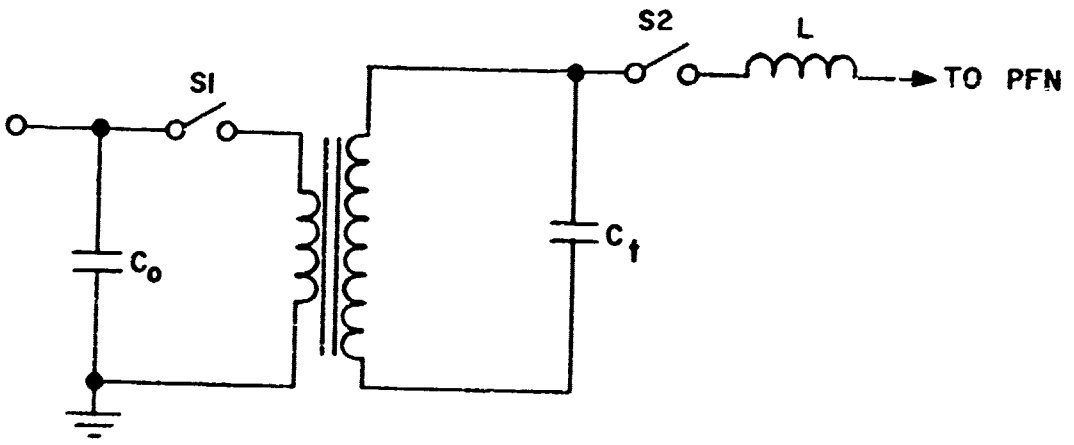

(b) SINGLE PULSE CHARGING

FIGURE 7

PULSE TRANSFORMER CHARGING SCHEMES

in 10 ns burst requires a PFN capable of producing input pulse energy in the range of 0.25 to 2.5 joules per pulse. At the design impedance of 17 ohms selected for the breadboard Travatron the traveling wave height produced by the PFN must be approximately in the range of 30 to 90 KV. If the PFN is a simple charged line, the resonant transfer circuit must provide charge voltages up to 180 KV while only 90 KV is required if the PFN is a Blumlein. Either PFN can be accommodated reasonably if the transfer capacitor C_t is charged to approximately 100 KV. To meet the energy requirement, C_t must be approximately 500 pf.

An important consideration in the design of the pulse transformer is the required weight and size as determined primarily by the peak voltage required and the energy handling. The ideal pulse transformer neither stores nor dissipates energy. However, in the practical case, the energy handling capability of the core can be estimated by a formula due to Bostick[5] which states:

$$W_d = \frac{10^{-6}(\Delta B)^2}{4\pi \mu_e} \tag{29}$$

where W_d is the energy density in joules/cm^3, ΔB is the peak flux density in the core above the remanent value in gauss. Typically, $\Delta B = 10^4 B$ gauss, and $\mu_e = 100$ for laminated iron cores. Then $W_d = 10^{-1}$ joules/cm^3. If energy handling were the only consideration in designing pulse transformers for the Travatron modulator, very small cores could be used and no particular advantage in this regard would be served by step-charging over single pulse charging.

Voltage handling needs are similar for both transformer types illustrated in Figure 7. At the 100 KV level the margins required to prevent breakdown (between windings and between the secondary and core) lead to considerably greater core volume than that suggested by energy handling.

b. Breadboard Models

The above considerations suggest that the technique of step-wise charging provides no real savings in size and weight since these parameters

are governed largely by peak output voltage. However, the technique does allow for rather modest energy and voltage handling in the primary circuit which can, therefore, be of all solid state design. To evaluate the method a capacity discharge ignition system* was used with both standard and special high voltage output coils. Holding diode D in Figure 7 was made up of a stack of three Unitrode USR 120 diodes, each rated at 12 KV. This limited the output voltage on C_t to less than 40 KV. However, the level was sufficient for evaluation of the technique. The Mercury system was capable of transferring approximately 30 millijoules per pulse. In the breadboard circuitry C_t had a value of 180 pf, thereby requiring four to five steps to reach a full charge near 40 KV. With the primary circuit operating at a repetition rate of 100 Hz, the transfer capacitance was charged in 50 μs whereupon it discharged through the spark gap switch S_2 at a 20 Hz rate.

The initial promise of the step charge method was overshadowed by difficulties in achieving substantially higher primary circuit repetition rates and by high voltage failures in the output transformer which was not intended for this service. Presumably these problems are straightforwardly solvable. However, efforts to achieve single pulse charging at full voltage and energy were highly successful and this latter method was adopted for the remainder of the program.

The single pulse charging circuit of Figure 7 was implemented as shown in Figure 8. The primary circuit consists of a 2 μf, 2 KV capacitor discharged through the primary of the transformer by means of a triggered spark gap (EGG Model GP113). A trigger circuit similar to one used by Moriarty et al[6] was constructed using 10 SCR stages to provide the necessary trigger signals. A timing circuit was built to drive the trigger pulser at repetition rates up to 1000 Hz.

The transformer providing a 50:1 voltage step-up employed a laminated iron core. The primary was wound in one layer, the secondary in several layers separated by Mylar. Design considerations aimed at

---

*Mercury Thunderbolt Ignition System

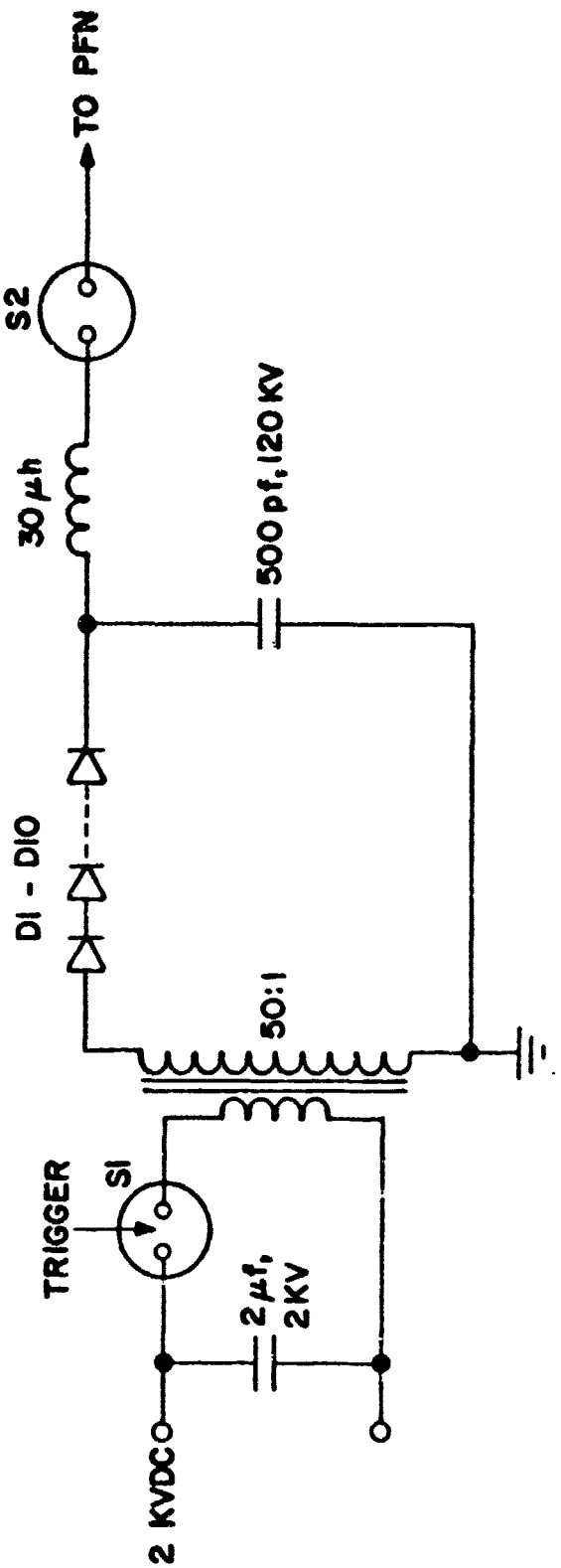

FIGURE 8

BREADBOARD PULSE TRANSFORMER CIRCUIT

providing sufficient spacing for 100 KV output led to a core volume of approximately 200 cm^3. The wound core was packaged in an oil filled steel housing having a volume of about 0.13 $ft.^3$ and a weight of 10 lbs. The unit was capable of steady state operation at a repetition rate of 100 Hz.

A diode stack employing 10 Unitrode USR 120 diodes was used to isolate the 500 pf transfer capacitor from the transformer and to ensure a sufficient time for breakdown of the over-volted, pressurized spark gap S_2 in the transfer circuit. The transfer capacitor consisted of a series-parallel arrangement of sixteen 500 pf, 30 KV capacitors.

The pulse transformer circuit performed successfully with the transfer circuits and PFN's used throughout the program. It provided considerable flexibility in achieving various pulse heights and repetition rates and exhibited an efficiency of approximately 70%.

4. PIEZOELECTRIC PULSER

a. General Background

As is well known, the piezoelectric effect is exhibited in certain natural crystals wherein a mechanical stress or strain in the crystal produces an electric field and visa versa. The effect in crystals such as quartz and Rochelle salt is a very small one and, as a result, applications using these materials have been restricted to frequency stabilization, microphone uses and in underwater sound transducers. Recent advances in the inducement of the piezoelectric effect in certain polycrystalline ceramics has permitted much larger coefficients. Indeed, ceramic crystals formulated from lead zirconate-titanate are now used commercially in spark generators in which voltages of many kilovolts can be generated.

Typical of such generators is Clevite's "spark pump"[7] used for ignition purposes. It is constructed of two ceramic slugs 3/8" in diameter by 3/4" long arranged mechanically in series and connected electrically in parallel. The device is operated by a cam driver which exerts a force corresponding to 7000 PSI in the ceramic. Potentials up to about 20 KV are

produced on the 80 pf capacitance of the parallel ceramics.

In application to the modulator needs for the Travatron, such devices, when scaled to higher voltage and energy, appear to be well matched to the need for large peak power and low duty cycle. The electrical energy stored in the piezoelectric ceramic can be discharged rapidly into the Travatron PFN which may therefore be viewed as C_t in Figure 6 above. The piezoelectric ceramic is well suited to this role in that the material is an excellent dielectric in terms of its high dielectric constant and low internal leakage. The piezoelectric generator also offers a variety of possibilities for direct mechanical-electrical energy conversion where the electrical energy is developed in a form directly useful for fast, high power discharge application.

To illustrate the utility of the piezoelectric generator, a breadboard model was constructed in the program using a series parallel stack of ceramic elements. Mechanical energy was delivered hydraulically from a high pressure gas source serving as the energy storage device. Because a limited number of elements were used, the breadboard model was not capable of the high voltage operation needed in further breadboarding of the Travatron system in this program. However, sufficient apparatus was assembled to show that higher voltage, higher energy devices are clearly possible. Moreover, the use of pressurized gas as an energy storage scheme was also successfully illustrated.

b. Piezoelectric Parameters

The piezoelectric effect arises in any asymmetric crystal where applied mechanical forces result in charge separation through crystal deformation. In general, one must be concerned with the full tensor properties of such crystals. However, in the following only the longitudinal (Z-axis) behavior is of interest where the electric fields are generated by stresses along a common axis.

The equivalent circuit for a piezoelectric generator is illustrated in Figure 9. The stressed crystal is represented by a voltage source in series with a capacitance shunted by a resistance corresponding to the internal

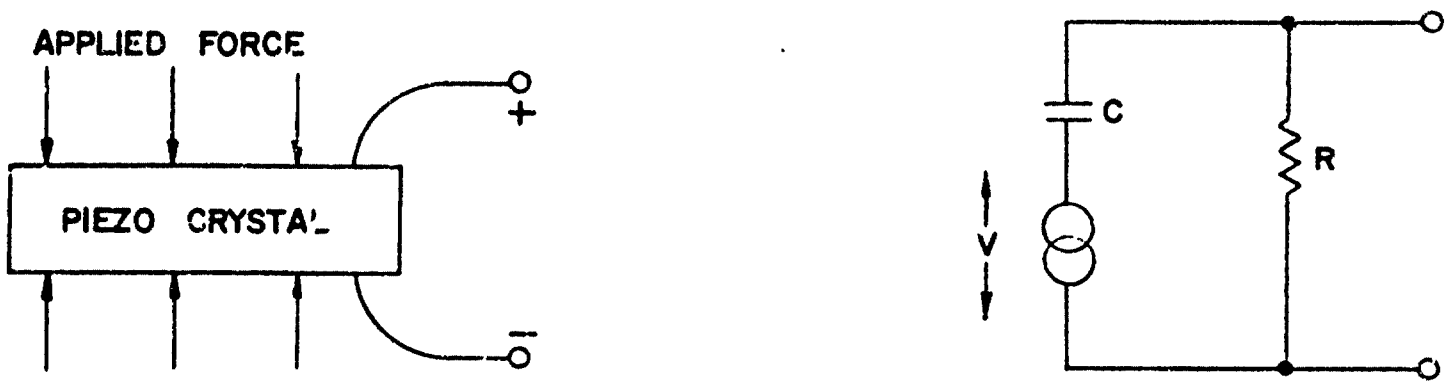

FIGURE 9

EQUIVALENT CIRCUIT OF A PIEZOELECTRIC GENERATOR

leakage resistance of the ceramic. Generally this resistance is very large (typically 10^{12} ohms or greater) and may be ignored.

Of particular interest for use in high voltage generation is a ceramic known as PZT-4 in view of its large piezoelectric constant g_{33} defined as the ratio of open circuit field to the applied stress. For PZT-4:

$$g_{33} = 24.9 \times 10^{-3} \text{ volts m/Newton}$$

$$= 4.4 \text{ volts/in/PSI} \tag{30}$$

The maximum stress which may be applied without degradation of the piezoelectric properties of the ceramic is approximately 10,000 PSI corresponding to a maximum electric stress of 44 KV/in. The constant d_{33} is defined as the ratio of strain developed to the electric field which for PZT-4 is:

$$d_{33} = 285 \times 10^{-12} \text{ meters/volt}$$

$$= 1.12 \times 10^{-8} \text{ in/volt} \tag{31}$$

The electromechanical coupling coefficient k_{33} is defined as the square root of the ratio of electrical energy stored to mechanical energy applied. Thus, the efficiency is given by k_{33}^2, which for PZT-4 is:

$$k_{33}^2 = 0.49 \tag{32}$$

Finally, the effective relative dielectric constant K_{33} is of interest. For PZT-4:

$$K_{33} = 1300 \tag{33}$$

The above parameters are sufficient for the basic electro-mechanical design of a pulser. For example, if it is desired to generate a peak voltage of 100 KV in a single ceramic with 10^4 PSI applied, the thickness must be 2.27 in. If a capacitance of 500 pf is desired, then the stressed area must be approximately 3.88 in^2. The volume of material is then 8.8 in^3 and energy is stored at a maximum energy density of 0.28 joules/in^3.

c. Pressure Vessel as an Energy Storage Device

The requirement for large stresses and small displacement for activating a piezoelectric generator can be obtained in a variety of ways employing well known hydraulic techniques. Perhaps the most interesting method from the point of view of energy storage is that employing a high pressure gas vessel with direct valving to the piezo element. Such a system is illustrated schematically in Figure 10. Gas pressure is alternately applied to the piezo and released by the fill and release valves respectively as indicated in the figure. The energy storage density in the pressure vessel is considerable as may be estimated by the isothermal compression of an ideal gas. The work done, and therefore the energy stored, in such a compression is given by:

$$W_d = RT_o \ln V_o/V_f \tag{34}$$

where

R = 8.3 joules/mol ^oK

$T_o \doteq 300^oK$ at STP

V_f = final volume

V_o = initial volume

For air compressed to 10,000 PSI, the energy stored is, approximately:

$$W_d = 0.49 \text{ kilojoules/gm} = 240 \text{ kilojoules/liter} \tag{35}$$

Continuing the above example wherein the piezo generates 2.5 joule/pulse, the gas consumption at 100 pulses/sec would be only 2 cm^3/sec. Energy storage by this means has many obvious advantages. The storage energy density is very high and, in fact, approaches high explosive values. Moreover, the form of the energy is much more passive in nature than is the case with either electrical or chemical storage. Its primary disadvantage lies in the relatively modest rates of extraction that are possible.

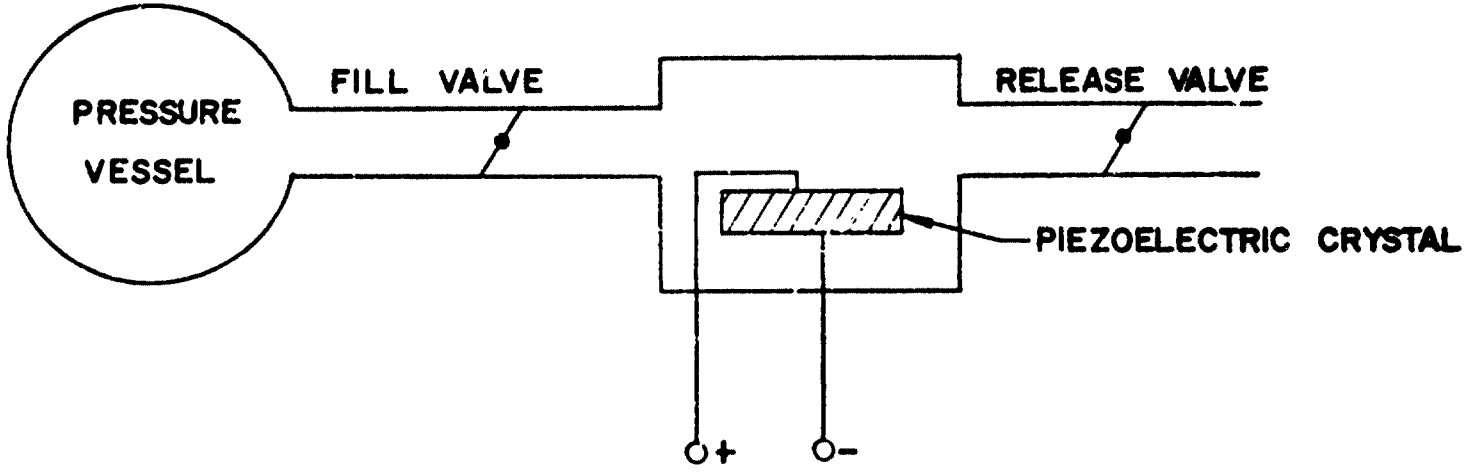

FIGURE 10

PIEZOELECTRIC GENERATOR WITH PRESSURE VESSEL ENERGY SOURCE

d. Breadboard Model

A working breadboard model of a piezoelectric high voltage generator was built and tested as a part of the effort in this program. A schematic of the generator and test set-up is illustrated in Figure 11. A 3-way solenoid operated valve* alternately applies pressure to the piezo stack and vents to atmosphere as controlled by a solenoid driver supplying, typically 24 vdc, 1 amp pulses. The gas source is a standard compressed air cylinder providing regulated pressure up to 2000 PSIG. At peak voltage, the energy stored in the piezo stack is discharged through the spark gap switch, a series inductor and a capacitor whose value was chosen to match that of the piezo.

The mechanical design of the generator is shown in the cross section of Figure 12. Air pressure applied at the input by the SV 10 valve creates a pressure on the steel piston which intensifies the pressure on the piezo stack by a factor of five, the ratio of piston-to-piezo area. The piezo stack is compressed against the lucite plate which also serves as an insulator for the high voltage side of the stack. The upper side of the stack is grounded through the steel piston and conducting "0" rings to the body of the generator.

The piezo element in the generator is a stack of two 3/8" thick rings having a 2" ID with 3" OD. The rings are segmented into four sections (to relieve hoop stress when compressed) as seen in the photo (Figure 13) of the disassembled device. The material is PZT-4, silvered on both sides. The capacitance of the assembled stack is 1500 pf and the maximum voltage at 10,000 PSI is 33 KV. This model could readily be extended to a 100 KV, 500 pf device by utilizing a total of six rings identical to those used in the breadboard.

---

*Victor Controls Series SV 10

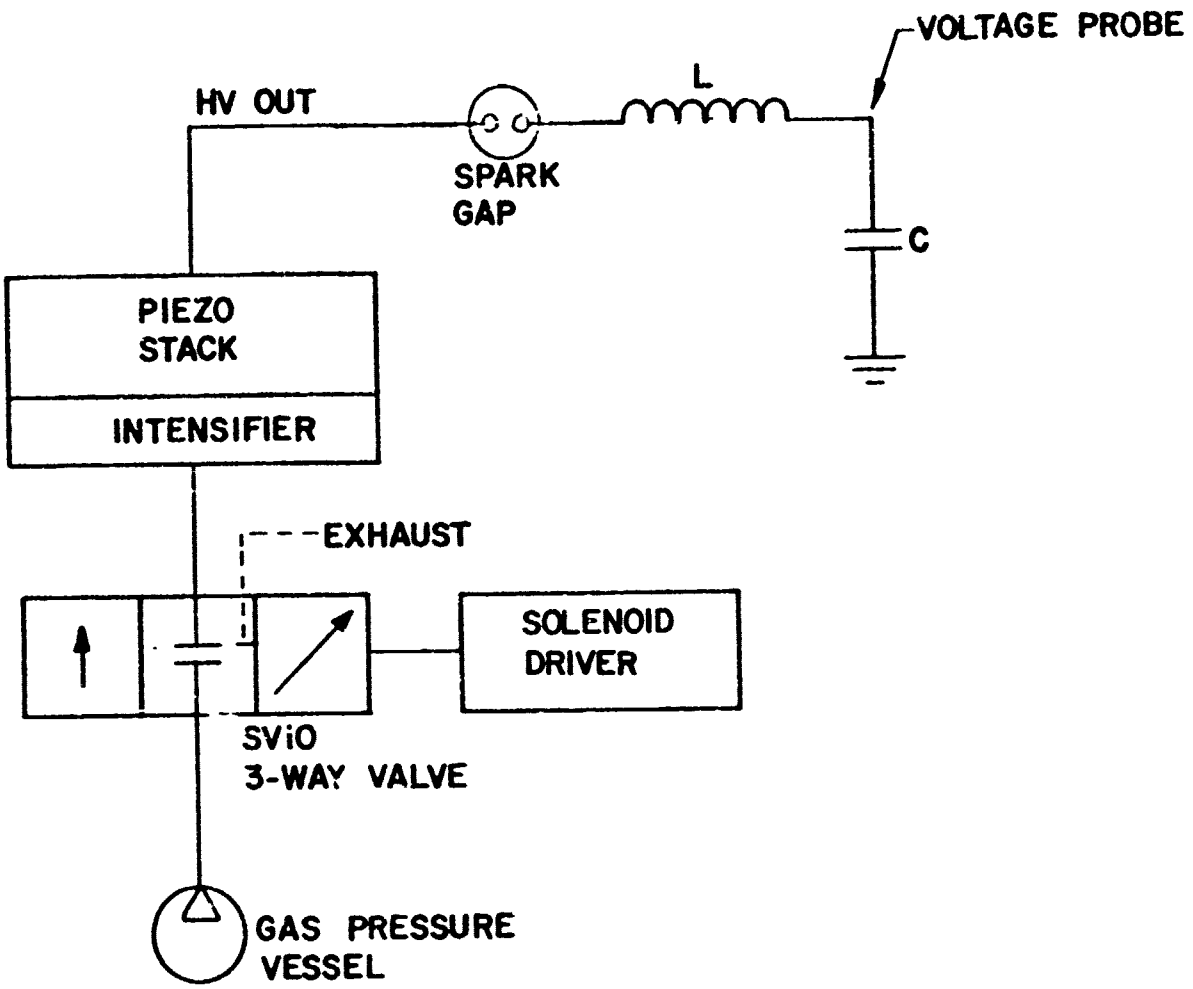

FIGURE II

PIEZOELECTRIC BREADBOARD MODEL SCHEMATIC

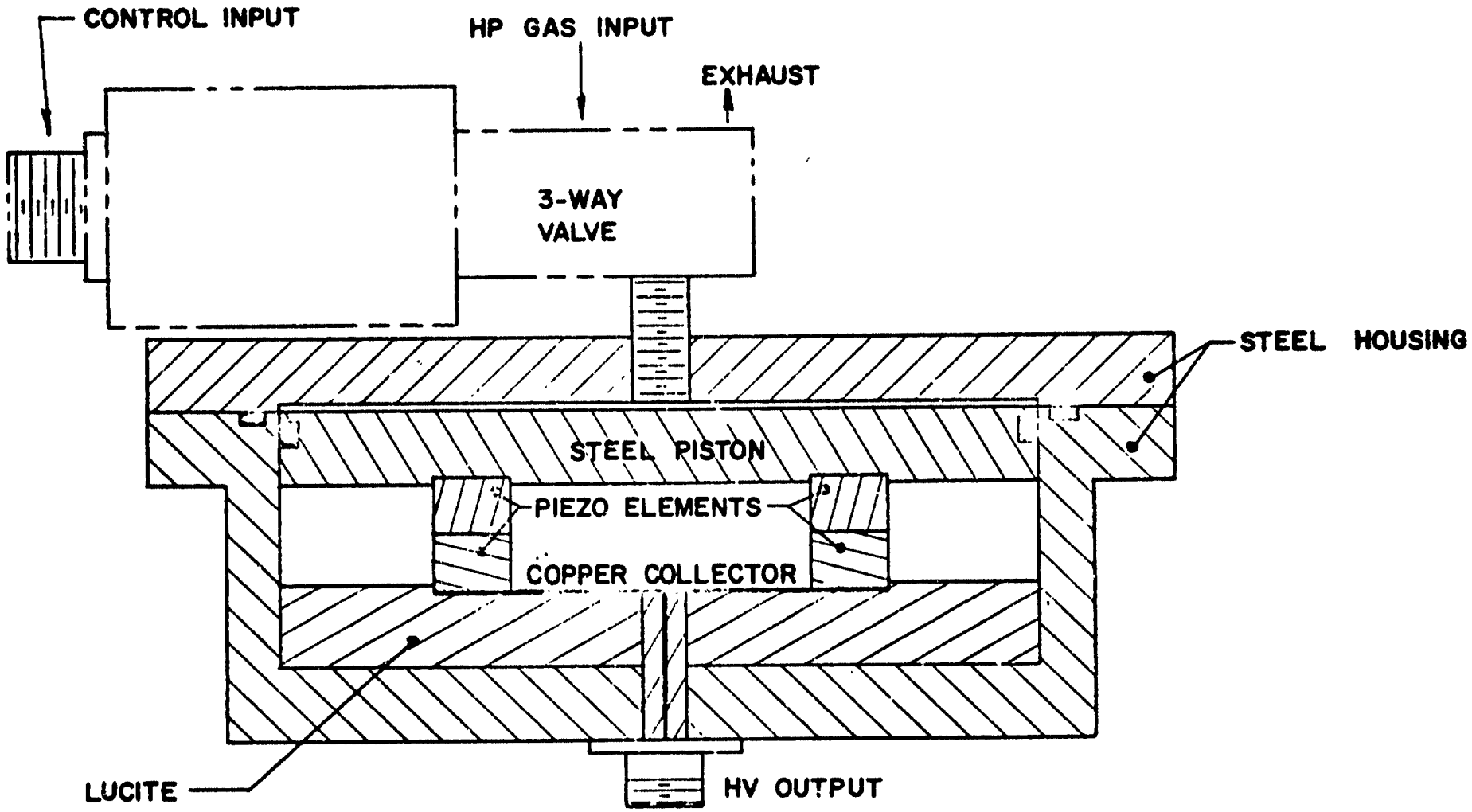

FIGURE 12

PIEZOELECTRIC GENERATOR

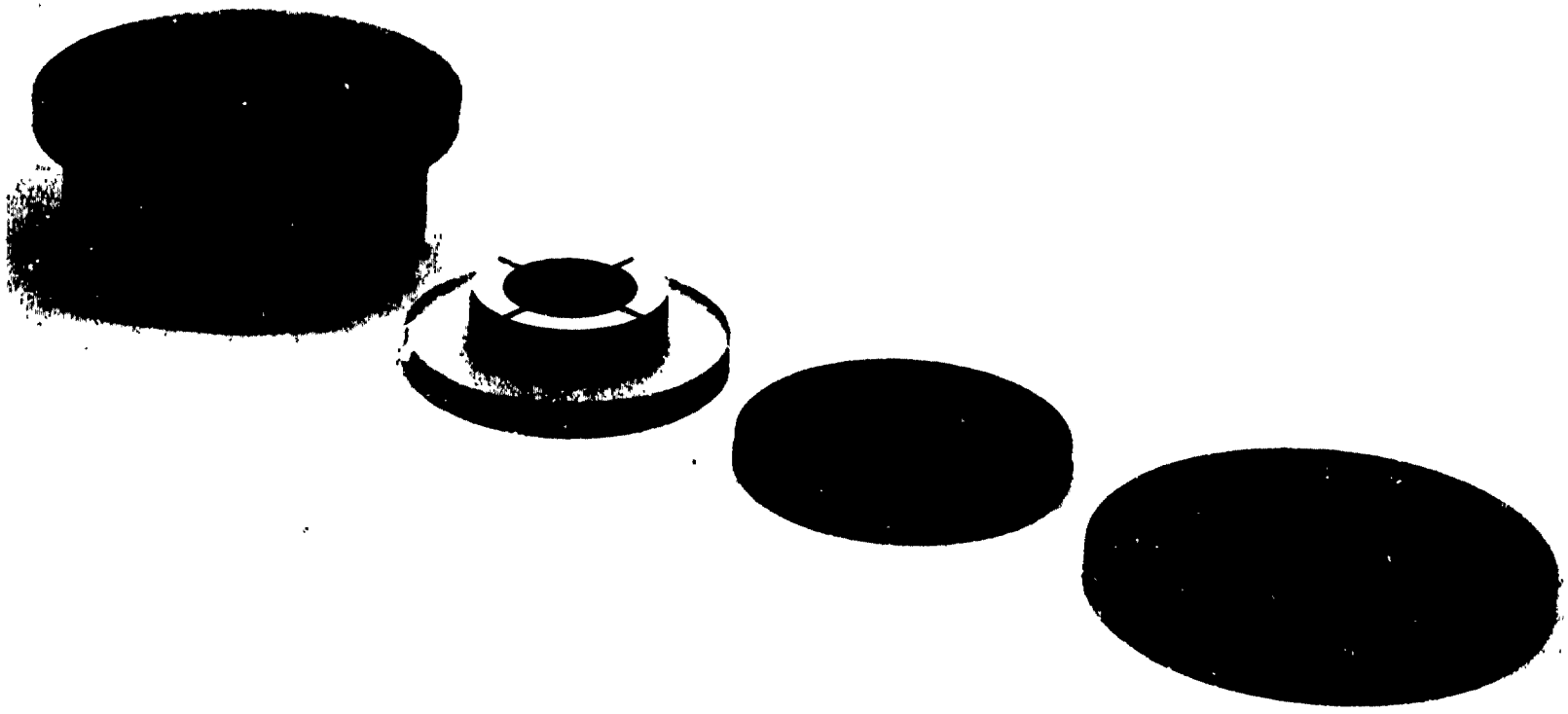

FIGURE 13

HIGH VOLTAGE PIEZOELECTRIC GENERATOR

In testing the device, it was used as the primary capacitor C_t in a resonant charging scheme (see Figures 6 and 11). A simple adjustable air gap was used to switch the output at peak charge voltage through a 15u h inductor and 1500 pf capacitor. The voltage waveform on the load capacitor was monitored through a high voltage probe. A series of tests were run with the driving pressure between 400 and 1200 PSI. The waveform reached a maximum voltage in approximately 200 ns followed by a slowly damped oscillation. The peak voltage was approximately 80% of the theoretical value for the pressure used in each case. The highest voltage attained was 16 KV at an operating pressure of 1200 PSI. This corresponds to a stored energy of 0.19 joules/pulse. At the design limit of 2000 PSI (before intensification) the energy stored by the test piezo stack could reach approximately 0.8 joules.

Pulse repetition rates were limited by the pneumatic time constants of the system to about 10 pulses per second. The gas filled volume of such a generator could be greatly reduced below that used and the time constants could approach that of the valve actuation time. The SV 10 has a rated response time of 15 ms.

5. SPIRAL LINE PULSE GENERATOR

a. Background

A spiral line pulse generator[8] is a field reversal device which affords a large pulse voltage step-up without recourse to heavy iron cores characteristic of the pulse transformer. While its directly generated pulse shape is not useful as the modulator input to a Travatron the spiral line pulser is an interesting candidate for pulse charging the PFN as described above. A breadboard model was therefore fabricated for evaluation in this program.

The basic generator is constructed by winding a stripline into a spiral coil as indicated in Figure 14. Insulation between turns is similar to that of the original line. The stripline is then charged to an initial potential V_o and a fast shorting switch is placed across the line, in this

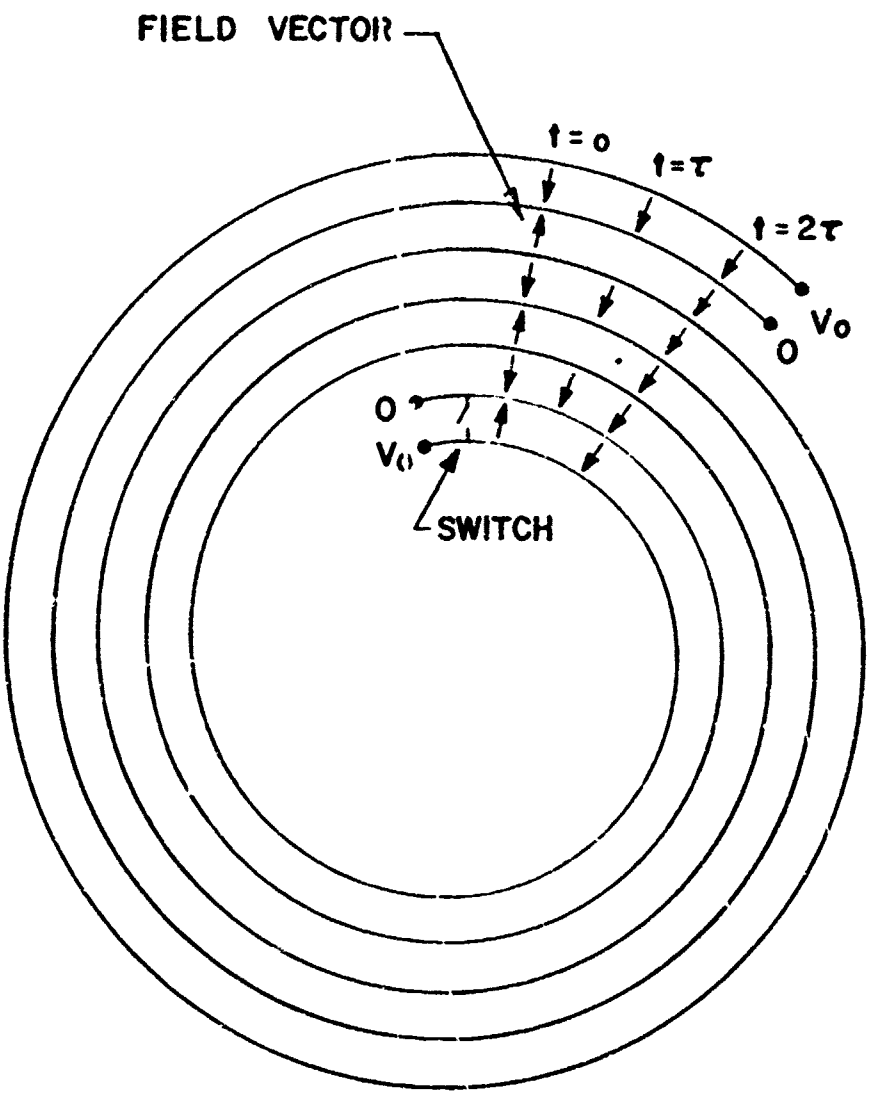

FIGURE 14

SPIRAL LINE PULSE GENERATOR SCHEMATIC

case at the center of the winding. The spiral coil now consists of an active line supporting propagating waves and a passive line which is unaffected by the switch function.

In the initial state, the field vectors are all opposed such that there is no potential drop between inner and outer conductors. When the switch is closed the electrostatic condition in the active line is replaced by a propagating electromagnetic wave which effectively cancels the vectors in the line in a progressive manner. Ideally, the potential between inner and outer conductors builds up to nV_o at the end of one transit time τ in the active line. At this point the traveling wave encounters an open and reflects in phase such that the wave vectors add to the electrostatic vectors of the passive line. Thus, the potential continues to increase reaching a maximum at $t = 2\tau$ and subsequently decreases. The theoretical pulse voltage waveform is given by:

$$V(t) = nt/\tau \cdot V_o \qquad 0<t<2\tau \qquad (36)$$

$$V(t) = 2n\left(1 - \frac{t - 2\tau}{2\tau}\right) V_o \qquad 2\tau<t<4\tau \qquad (37)$$

where

$$\tau = n \pi D/v \qquad (38)$$

D = diameter of spiral line

v = velocity of propagation in the line

The waveform is therefore ideally a triangular wave having a maximum value of $2nV_o$ at $t = 2\tau$. At that time the system is effectively 2n coaxial capacitors in series with each capacitor charged to V_o. The output capacity is therefore

$$C = (2n)^{-2} C_o \qquad (39)$$

where

$$C_o = n\pi D\ell\epsilon/d \quad (40)$$

ℓ = height of spiral line

d = spacing between conductors

ϵ = dielectric constant of the insulator

A number of loss mechanisms affect the waveshape in practice and the maximum voltage obtainable. Fitch et al[8] has defined several loss factors such that

$$V_{max} = 2n\beta V_o \quad (41)$$

and

$$\beta = \beta_1 \beta_2 \beta_3 \quad (42)$$

where:

β_1 = switch inductance factor

β_2 = risetime loss factor

β_3 = inductive coupling factor

When the rise time of the switch is very small compared to the transit time in the spiral line, β_1 approaches unity. Similarly, β_2 is close to unity when losses associated with insulators and conductors in the strip line are small. The inductive coupling factor β_3 is near unity if the ratio D/nd is large. Thus, a large diameter spiral compared to the build-up height of the line is required.

b. Breadboard Model

A breadboard model of a spiral line was constructed as a part of the program effort to permit an evaluation of the generator as a possible candidate pulse voltage source. A nominal one joule device was constructed using n = 6, D = 9" and ℓ = 6". A polyethylene dielectric was used having a thickness of 35 mils and a relative dielectric constant of 2.2. With a charge voltage of 10 KV, the theoretical peak output voltage from equation (41) is:

$$V_{max} = 1.2 \times 10^5 \ \beta \text{ (volts)}$$

and the output capacitance from equation (40) is:

$$C = 100 \text{ pf}$$

The transit time from (38) is:

$$\tau = 18 \text{ ns}$$

The switch used in the breadboard model was a pressurized triggered spark gap having a rise time of approximately 1 ns. From reference 8, the switch inductance factor β_1 can be calculated with the result that $\beta_1 = 0.93$. The rise time loss has also been tabulated. For the copper conductors used, $\beta_2 = 0.98$, while $\beta_3 = 0.90$. From (42), the overall loss factor is then estimated to be: $\beta = 0.82$. Thus, when $V_o = 10$ KV a peak output voltage of 98 KV was expected for the breadboard.

A photograph of the breadboard model is shown in Figure 15. The trigatron switch is seen in the right hand portion of the figure. Charging and trigger signal lines are shown as is the high pressure gas line. The high voltage output is extracted from the inside turn of the spiral coil.

Experimentation with this device was confirmed largely to observations of its peak operating voltage with the rationalle that if this parameter meets design expectation, then other parameters such as β and the basic functioning of the device must also be nominal. The measurement of peak output voltage was performed using a calibrated atmospheric spark gap. With a charge voltage of 10 KV, the output signal was determined to be 95 KV $\pm$ 5 KV in good agreement with the design value of 98 KV. The generator performed well without failure at this level for several hundred pulses at repetition rates below about 10 Hz. The primary concern regarding breakdown failure of the breadboard was in the area of the creapage margins at the coil ends. The dielectric volume stress was below 300 v/mil. If immersed in oil, it was estimated that the pulser could have operated at 20 KV input for nearly 200 KV output.

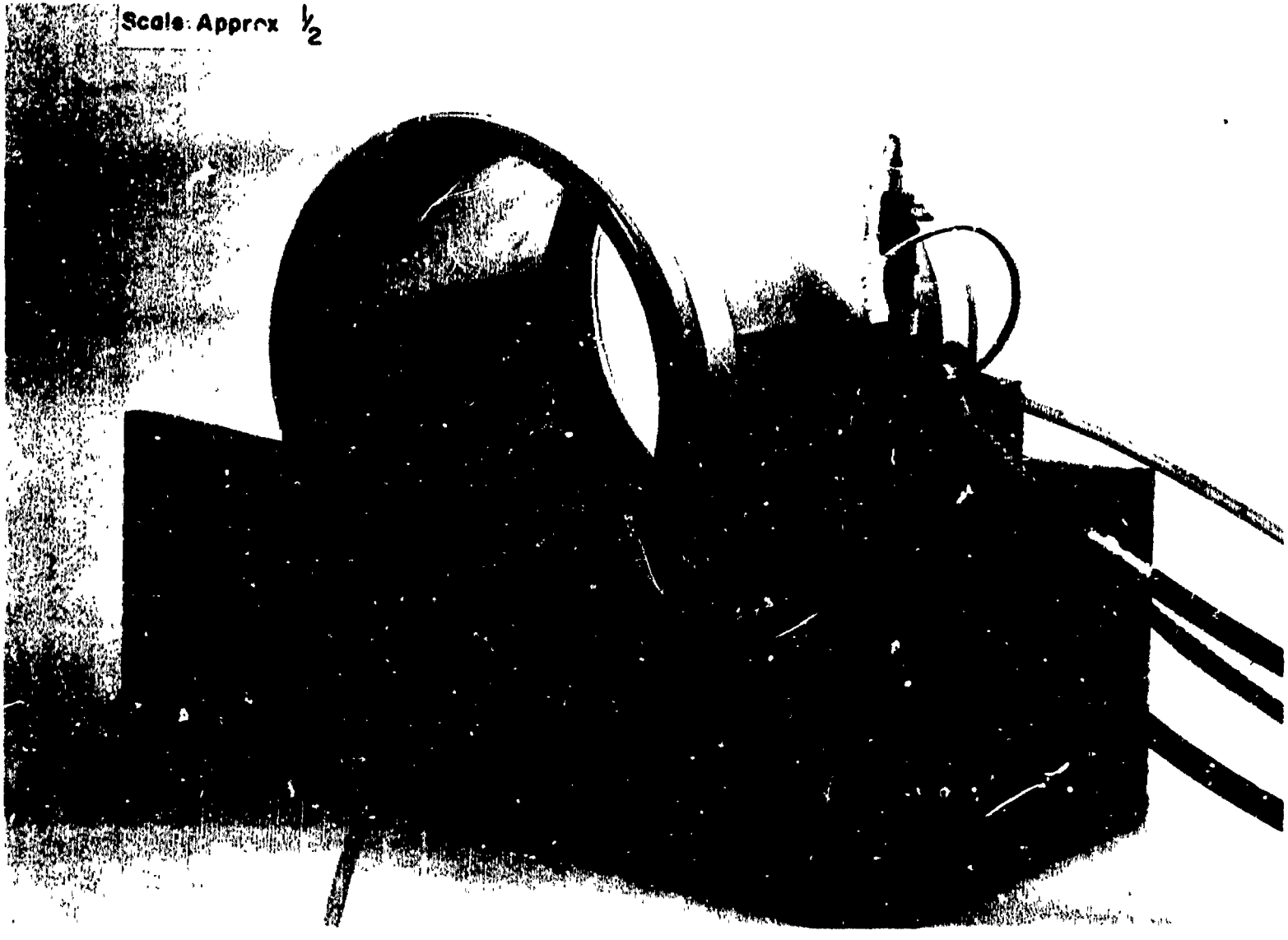

FIGURE 15

SPIRAL LINE GENERATOR

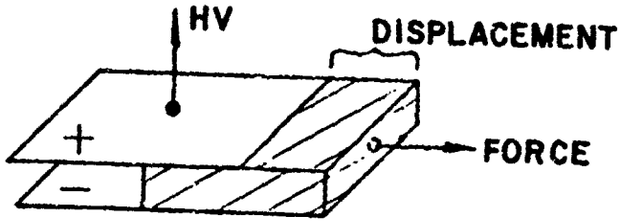

(a) DIELECTRIC MOTION

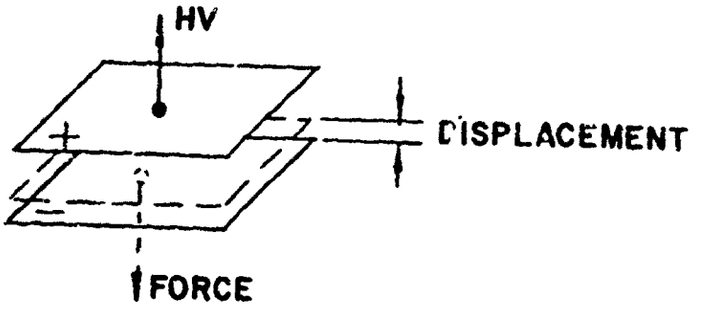

(b) PLATE SEPARATION

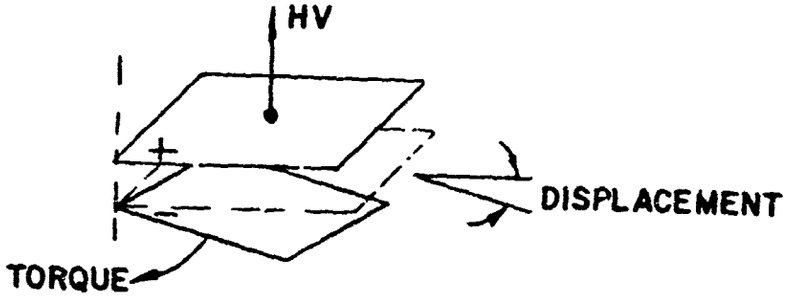

(c) PLATE ROTATION

FIGURE 16

SOME SIMPLE PARAMETRIC GENERATORS

The breadboard pulser was not used in conjunction with the breadboard Travatron largely in view of its modest output capacitance. However, the workability of the device at levels near the design values was clearly demonstrated lending confidence that future Travatron systems might successfully use generators of this type.

6. ALTERNATE SOURCES OF PULSED HIGH VOLTAGE

A portion of the program effort was directed to an assessment of other potentially useful sources of pulsed high voltage. Concentration was placed on two non-inductive techniques: (1) parametric devices involving time varying capacitance and (2) the Marx generator. Both of these generator types were judged to possess practical difficulties in implementation when linked to the pulse needs of the Travatron. For this reason no effort was applied to the physical design and construction of breadboard devices. The following paragraphs present a brief review of the design concepts.

a. Electrostatic Parametric Devices

Somewhat analagous to the magnetic alternator are the basic capacitive devices illustrated in Figure 16. In each case, a capacitor C_o is given an initial charge Q. The applied force and resulting mechanical displacement serve to reduce the capacitance of the system. The mechanical work is directly converted to electrical energy. If current does not flow the electrostatic energy and potential both increase by the same ratio:

$$E_f/E_o = V_f/V_o = C_o/C_f \qquad (43)$$

where the subscripts refer to the initial and final values.

From the standpoint of achieving large ratios C_o/C_f and of obtaining a rapidly repetitive function the scheme indicated in Figure 16(c) is perhaps the most attractive. Such a device has been studied by Brosan[9] and by Van de Graaff and Trump[10] in the form of a motor driven multipole, multiplate rotor revolving through a multiplate stator.

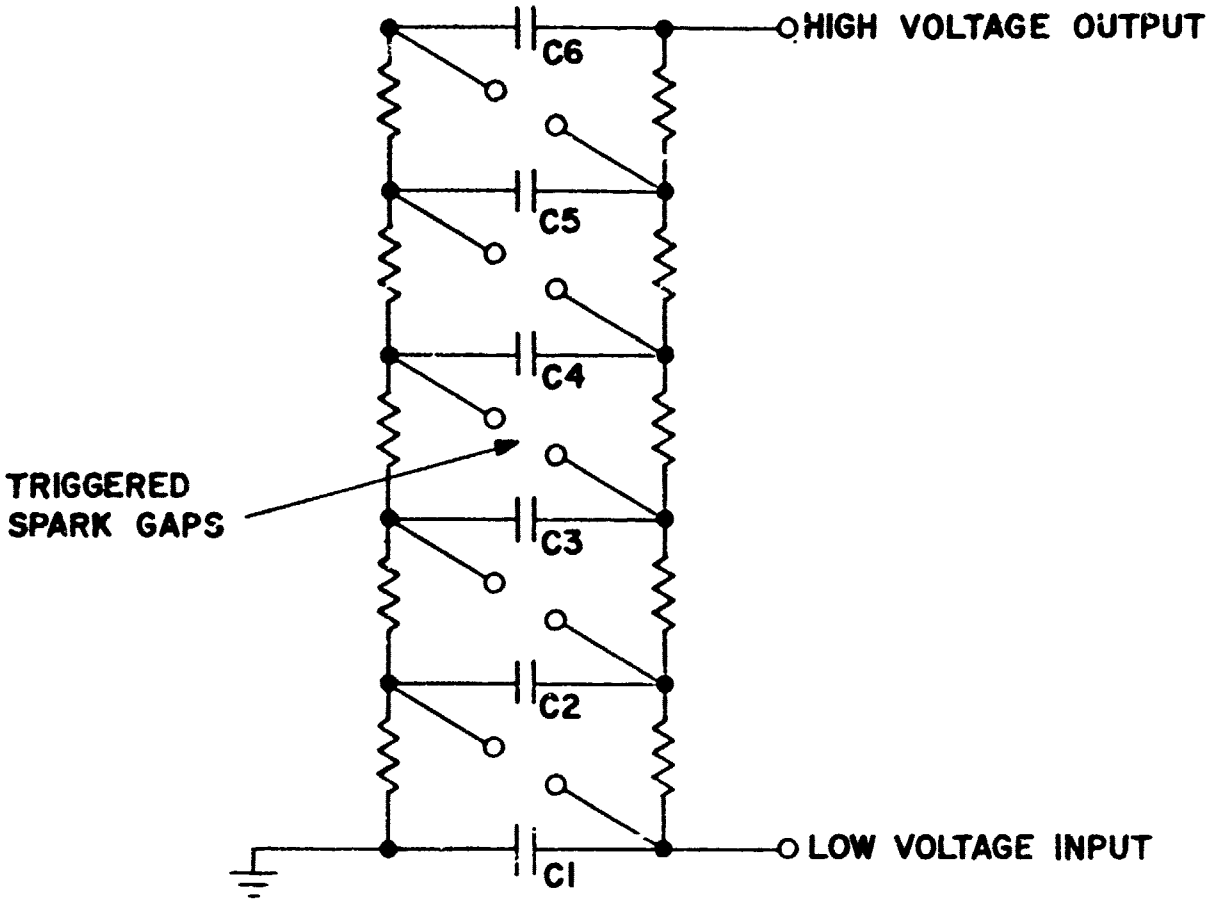

FIGURE 17

A MARX GENERATOR

This class of machine was analysed in the program effort to determine its utility to the pulse charging needs of the Travatron transmitter as outlined above. To this end the capacitance C_f was viewed as the transfer capacitance C_t (see Figure 6). Thus, in operation, as the rotor voltage builds up to its maximum value the rotor energy discharges through the transfer circuit to charge the PFN. Using nominal values considered above the machine must provide: C_f = 500 pf and V_f = 100 KV. Initial values C_o and V_o are somewhat arbitrary, but a voltage step-up of at least 10:1 might be considered desirable. The initial values of C_o and V_o would then be 5000 pf and 10 KV, respectively. The practical constraints begin at this point to preclude a realizable parametric generator having the desired performance characteristics. Because of the relative motion of the opposing plates of the capacitor and the high voltage present the dielectric must be considered a gas under pressure or a hard vacuum. In either case, spacings must be sufficient to withstand the final voltage. At the same time, a relatively large value of C_o (eg. 5000 pf) is required. Typically, for the required spacings needed the capacitance plate areas must be several square meters. Stacked arrangements of rotors and stators only compound the high voltage difficulties in view of the additional structure and supports. In view of these several serious fundamental design difficulties, further work toward breadboarding an operating device was not undertaken.

b. Marx Generator

The Marx generator is a conceptually simple pulse generating scheme (see Figure 17) whereby a number of capacitors are charged in parallel to some initial voltage V_o and subsequently discharged in series to produce an output voltage pulse of nV_o where n is the number of stages. The output capacitance is C_m/n where C_m is the capacitance of an individual element. In considering a design for possible use in the program effort, a ten stage Marx circuit was considered. To produce 100 KV pulses with an output capacitance of 500 pf, a charging voltage of 10 KV and capacitance per stage of 5000 pf would have been required. Such parameters appear quite tenable. However, a breadboard model was not undertaken in view of well known problems in attaining reliable operation.

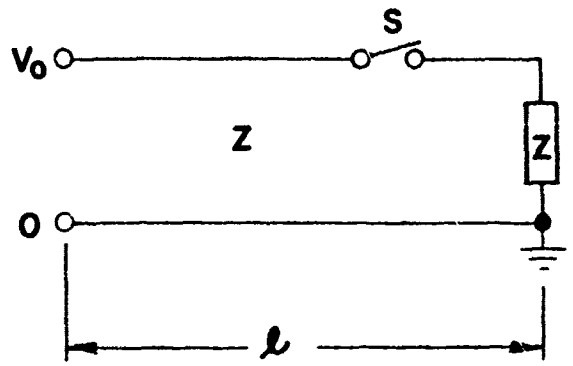

OUTPUT: $V = V_0 / 2$
$0 < t < 2\ell/v$

(a) DISTRIBUTED PARAMETER PFN

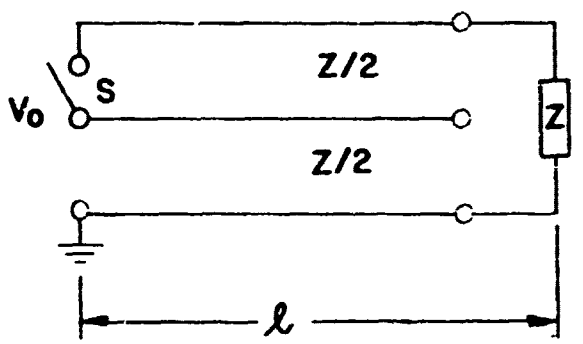

OUTPUT: $V = V_0$
$\ell/v < t < 3\ell/v$

(b) DISTRIBUTED PARAMETER BLUMLEIN

FIGURE 18

TRAVELING WAVE PULSE FORMING NETWORKS

These problems are associated largely with difficulties in obtaining correct synchronous spark switch operation, which in the present application are magnified by needs for long term repetitive performance.

7. PULSE FORMING NETWORKS

a. General Concepts

A pulse-forming network (PFN) is required to shape the high voltage pulses generated by the impulse charging scheme, typically of microsecond duration, to rectangular pulses of several nanoseconds width. The PFN can range from a simple charged transmission line to one of several types of vector inversion devices which provide voltage step-up simultaneously with the pulse-forming function. Although all PFN's have the same basic function, they differ in voltage input requirements, in input impedance and in overall complexity. Two devices employed in breadboard experimentation in this program were the coaxial line PFN and a triaxial Blumlein. Of particular interest in the program was the compatibility of the Blumlein device with the Travatron.

The basic operation of the two devices is indicated schematically in Figure 18. In the simple traveling wave PFN (Figure 18(a)) a voltage source initially charges a transmission line to a potential V_o. Upon closure of the fast switch S, a voltage pulse is delivered to the matched load Z having a pulse height $V_o/2$ and a duration $2l/v$ where v is the propagation velocity in the line. The Blumlein device is also a transmission line as illustrated in Figure 18b, but makes use of field reversal technique to produce pulse voltage step-up. Basically, transmission lines are charged in parallel and, by fast switching action, they are discharged in series such that their voltages and impedances add. In the form illustrated, two parallel transmission lines of impedance Z/2 are initially charged to V_o along a common conductor. The potential appearing across the load Z is initially zero because the field vectors in the two lines are in opposition. Following closure of the switch S, a vector reversing wave propagates toward Z such that the instantaneous potential across Z is V after a single transit time $2l/v$.

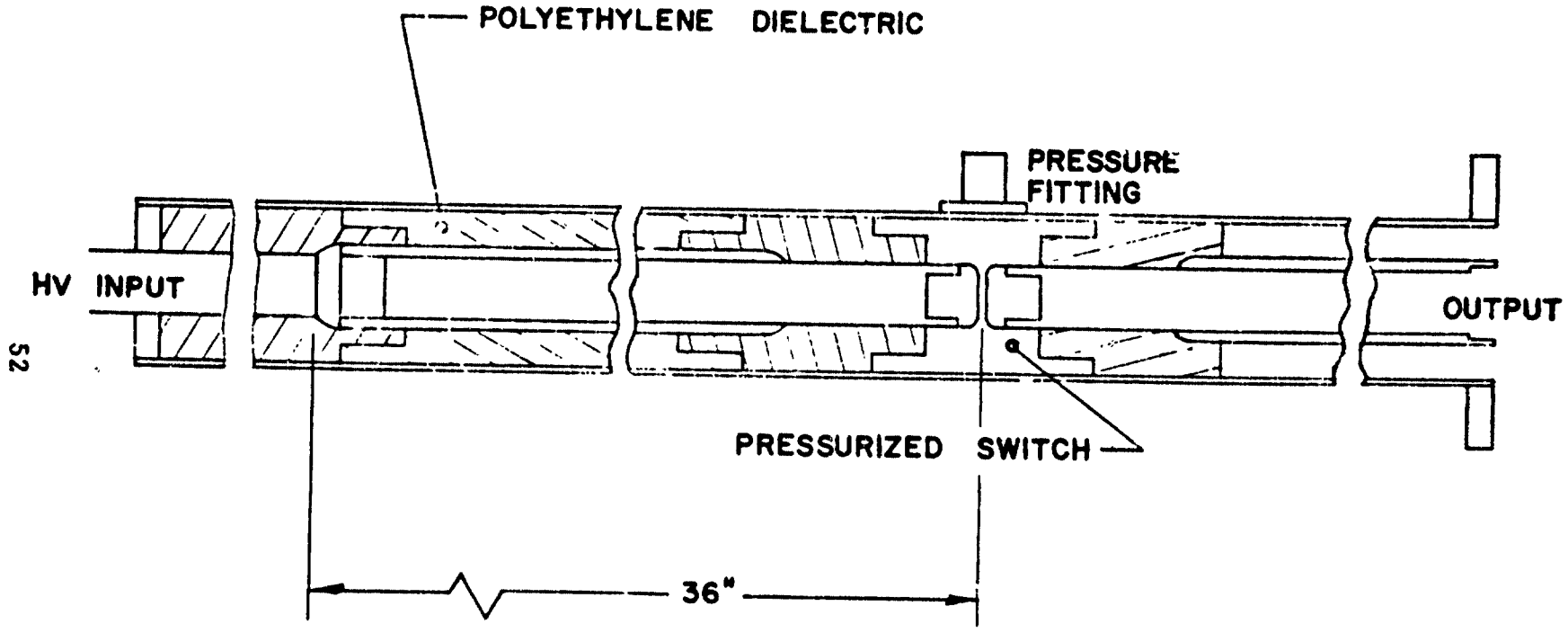

FIGURE 19

COAXIAL PFN

In effect, the electrostatic field in the upper line have been replaced by a propagating wave of opposite polarity. Current flows to the load as if from a transmission line of matched impedance until, after a two-way transit in the line, the potential across Z falls to zero. Consequently, the output pulse is identical to that from a single line of impedance Z charged to an initial voltage of $2V_o$.

b. Coaxial PFN

Considerable previous experience exists using the simple coaxial transmission line PFN. However, a breadboard model was constructed in the program effort to evaluate the resonant transfer technique described above and to ascertain that no new problems arise when the previous experience is applied to lower impedance configurations. As a by-product, the breadboard PFN was designed to match the initial test requirements of the breadboard Travatron. The PFN was, therefore, designed to provide a multi-kilovolt output in a matched 17 ohm load with a pulse width somewhat greater than 5 nanoseconds. Specifically, the basic design parameters were as follows:

Output Voltage: up to 50 KV
Output Impedance: 17 ohms
Pulse Width: 7.5 ns

The line was constructed as illustrated in Figure 19. The storage line employs a 1 5/8" OD outer conductor with a 1" OD inner conductor and polyethylene dielectric. The high pressure switch used to launch the traveling wave was designed for nanosecond risetime, achieved by relatively close gap spacing and large diameter electrodes. The switch dielectric was dry air at pressures up to about 200 PSIG. The line capacitance C_p is approximately 200 pf and is chargeable on a pulse basis to about 100 KV.

The test set-up used to test the basic PFN design is shown in Figure 20. The transfer capacitor C_t was chosen to have a value of 600 pf. A simple overvolted spark gap G_1 was used to transfer energy to the PFN with an expected voltage increase ratio of 1.5:1 according to equation (27). In typical operation, C_t was charged to 60 KV. The PFN was then resonantly

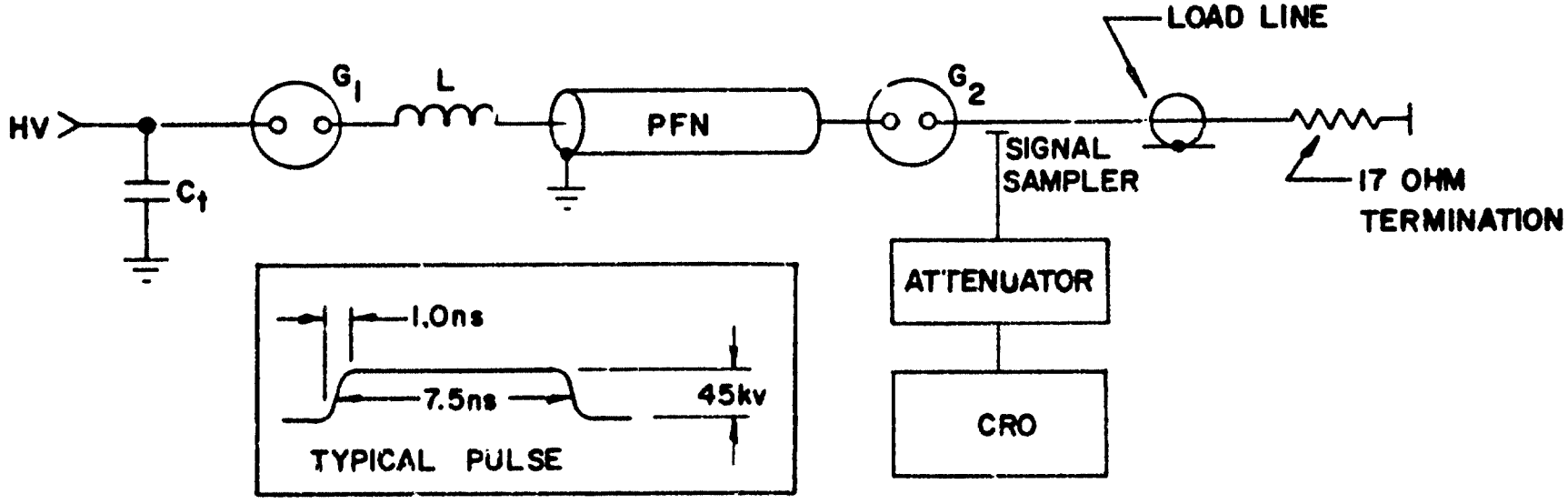

FIGURE 20

BASIC PFN TEST SET-UP

charged to 90 KV and a 45 KV pulse was launched into the matched load line. A wideband signal sampler employing capacity coupling was used to provide a calibrated output for observation on a travaling wave CRO. The typical pulse observed is indicated in the figure. Pulse heights observed were very close to nominal. The risetime was near one nanosecond under all operating conditions with output levels ranging from about 15 to 50 KV as determined by the pressurization applied to G_1 and G_2.

c. Triaxial Blumlein PFN

For generation of nanosecond duration pulses, a particularly useful embodiment of the Blumlein PFN is the triaxial form illustrated in Figure 21a. The innermost and outermost conductors are initially at ground potential while a third conductor, coaxial to both, is charged to a voltage V_o. A fast-acting switch is located as shown between the inner and intermediate conductor. Two coaxial lines are thus formed each having impedance Z/2 where Z is the output impedance.

The voltage doubling advantage of the Blumlein is obtained with the penalty of a prepulse, that is, a pulse which appears across the load prior to generation of the fast rectangular pulse. The prepulse arises during the impulse charging of the line due to capacity coupling as indicated in the equivalent circuit, Figure 21b. The prepulse problem is a well-known disadvantage of the Blumlein PFN, particularly in applications where the load is sensitive to voltage pulses prior to the main pulse. Such applications include field emission cathodes in flashX-ray machines, for example. In that case, the prepulse causes preionization of the region immediately adjacent to the cathode and seriously affects the character of the cathode current when the fast pulse arrives. Suppression of the prepulse can be approached in several ways and is frequently accomplished by some form of high-pass filter technique. The Travatron is extremely sensitive to prepulse effects since a long pulse of only a few kilovolts amplitude will prefire the switches in the traveling wave structure. Thus, when the fast pulse is launched, it finds each switch in a closed state and no reflections take p ace as required for proper function.

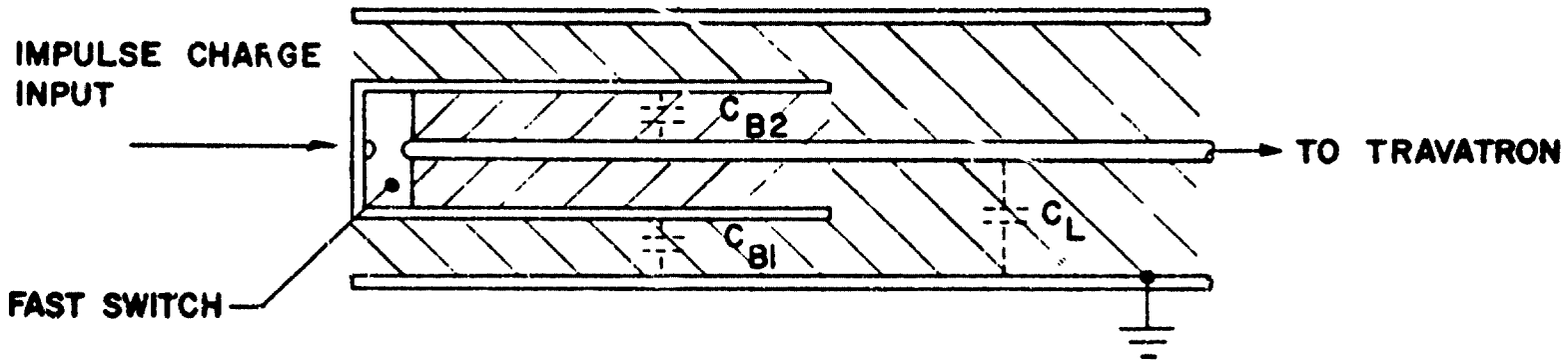

(a) SCHEMATIC OF TRIAXIAL BLUMLEIN

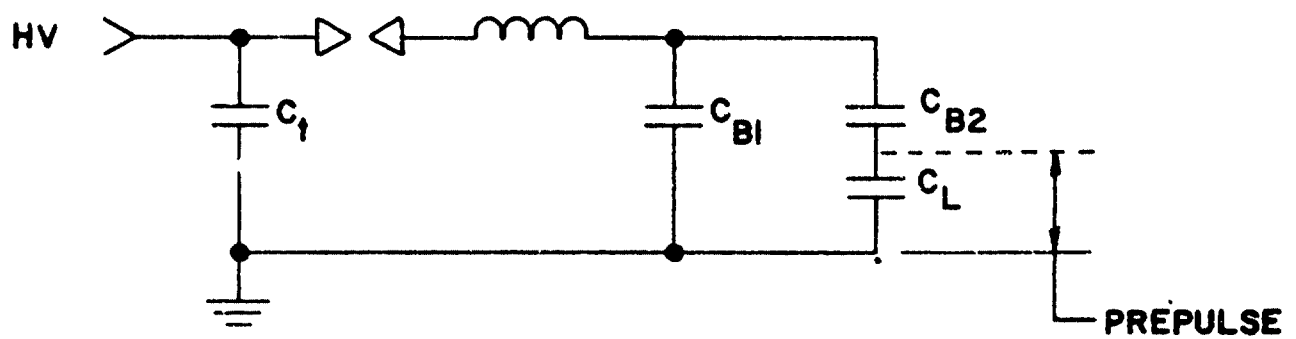

(b) EQUIVALENT CIRCUIT (CHARGING)

FIGURE 21

TRIAXIAL BLUMLEIN AND EQUIVALENT CHARGING CIRCUIT

The extent of the prepulse can be characterized quantitatively with reference to Figure 21b. During pulse charging the Blumlein and its associated output transmission line may be described by the three capacitances as indicated. C_{B1} and C_{B2} represent the capacitances of the two sections of Blumlein, while C_L is the capacitance of the interconnected line to the Travatron input and is effectively in series with C_{B2}. During pulse charging the potential appearing on C_L is:

$$V = \frac{C_{B2}}{C_L + C_{B1}} \tag{44}$$

where V_o is the peak Blumlein charge potential. If C_L is very small, $V \doteq V_o$ and the full charge potential appears across C_L even before the fast switch is closed.

In addition to the problem of prepulse voltage effects in the Travatron switching structure already described, other problems arise in connection with energy loss and adverse effects on the Blumlein switch which suffers a reduction in potential drop below the design value V_o.

From the equivalent circuit it can be shown that the energy coupled to the load by the prepulse E_L is related to the total energy stored within the Blumlein E_B by:

$$E_L/E_B = \frac{C_L C_{B2}}{2 (C_L + C_{B2})^2} \tag{45}$$

If, for example, $C_L = C_{B2}$, 1/8th of the energy is transferred to the load during the prepulse. From (44) the potential on C_L is $V_o/2$.

Another source of energy loss arises from the mismatch between C_t and the Blumlein during pulse transfer. Thus, the ideal transfer with $C_t = C_{B1} + C_{B2}$ cannot occur and the transfer charging efficiency will be less than 100%. Of the energy which is transferred, a fraction is not useful, having been lost to the load before the fast output pulse. Dynamically even more energy can be lost since the traveling wave launched by the fast switch is of reduced magnitude.

Several methods may be used to suppress the prepulse. Differing in complexity and effectiveness the methods all attempt to secure an effective ground reference for C_{B2} while blocking or preventing a voltage rise in C_L during the pulse charging of the line. In each case illustrated in Figure 22, a ground reference is maintained by an inductive path. The simplest method uses an inductive shunt chosen to provide a low impedance path during pulse charging and a high impedance path for the fast output pulse. To function the pulse charging time must be much longer than the output pulse, a condition which usually applies in order to assure uniform charging of the PFN before switching. Additional isolation of the load can be provided by the LC circuit of Figure 21b or by introducing a spark switch G as in 21c. The switch is designed to break down promptly when the fast pulse is incident but has a higher breakdown value than that fraction of prepulse which appears during charge transfer.

The experimental effort was undertaken to test the basic function of the triaxial Blumlein and to explore the extent and control of the prepulse problem. For this purpose, a Blumlein having a 50 ohm output was constructed as illustrated in Figure 23. The PFN employs a standard EIA 1 5/8" outer conductor with a standard output connector. The triaxial line employs teflon dielectric as indicated. The input contains the transfer inductor and a gas line for pressurization of the overvolted spark gap. The initial test set-up (Figure 24) was similar to that used to test the low impedance coaxial PFN described above. The Blumlein was resonantly charged from the 180 pf transfer capacitor through G_1 and an inductor chosen to provide a resonant transfer time of about 100 ns. The output was connected to a short section of terminated 59 ohm line. Because of the termination, the prepulse was expected to be very low and, in fact, not measurable in this setup. A calibrated signal coupler was employed to observe the output pulse. The typical pulse shape produced is illustrated in Figure 24. The peak voltage, 35 KV, was identical within experimental error to the high voltage charge potential placed on the matched charge transfer capacitor demonstrating the basic successful operation of the Blumlein. The pulse exhibited a fast rising portion to about 80% of its peak value followed by

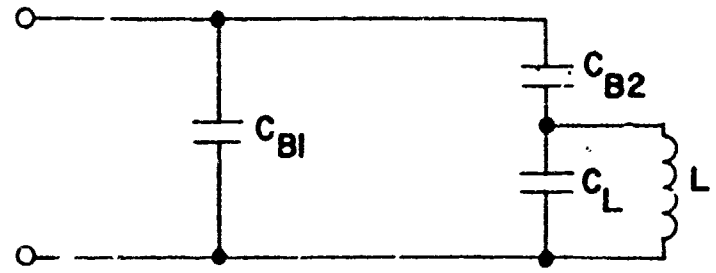

(a) INDUCTIVE SHUNT

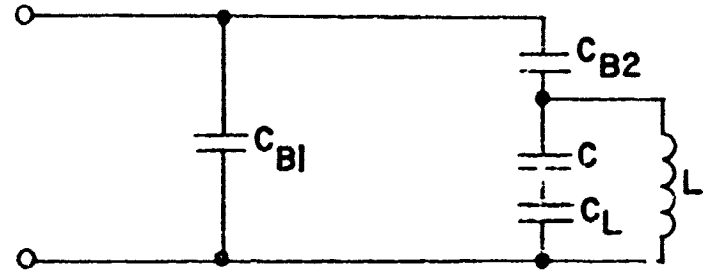

(b) HIGH PASS LC

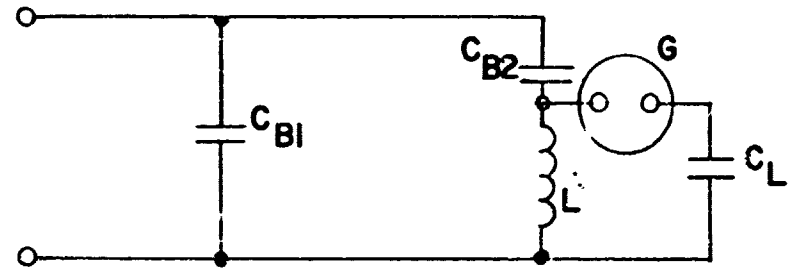

(c) INDUCTIVE SHUNT AND SPARK GAP

FIGURE 22

PREPULSE SUPPRESSION METHODS

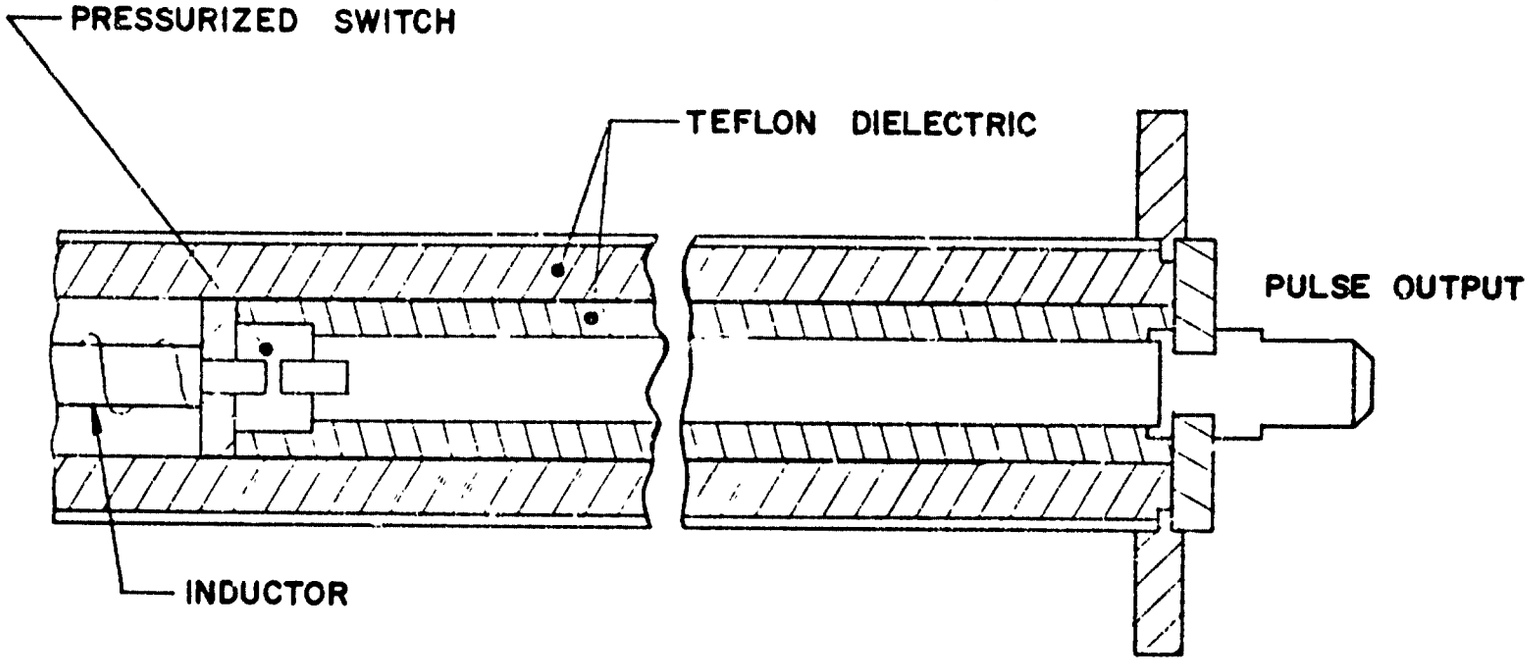

FIGURE 23

TRIAXIAL BLUMLEIN

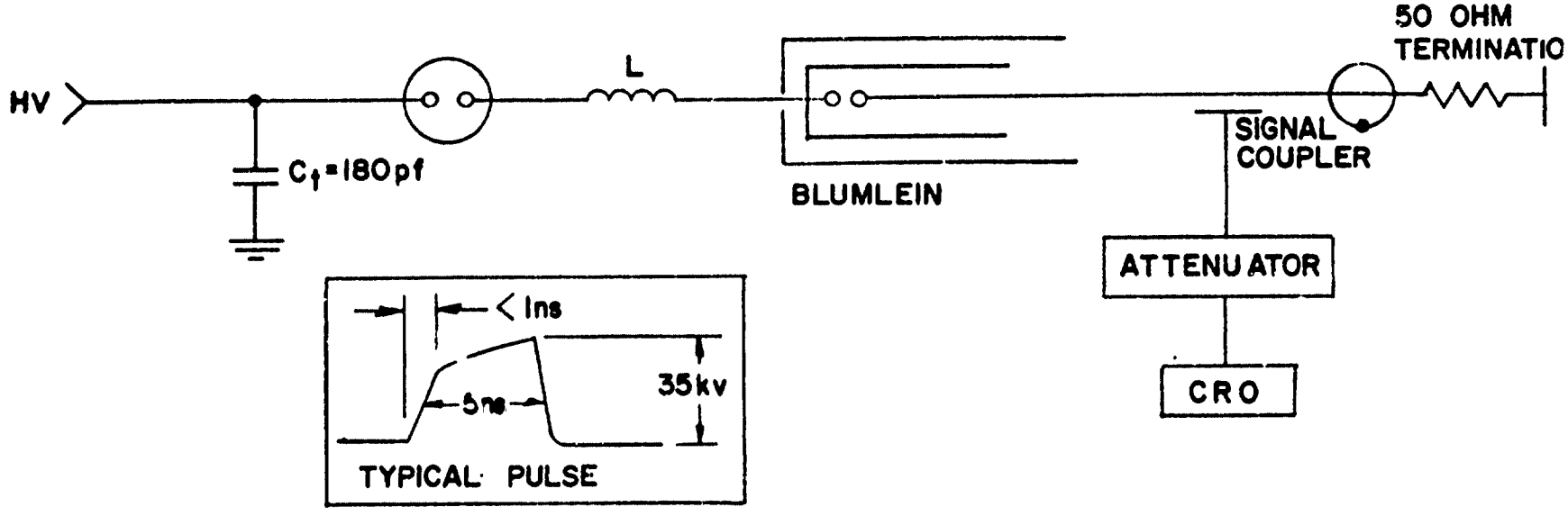

FIGURE 24

50 OHM BLUMLEIN TEST SET-UP

dribble-up to the full height. This was believed to be due to transmission line losses in the breadboard device.

In a subsequent series of experiments the extent of the prepulse was investigated, its effect on a spark gap switch at the output and means for prepulse suppression. To obtain a direct measurement of the prepulse a high voltage, high impedance (100 M ohm, 3 pf) probe was connected to an unterminated section of output line. The length of line was chosen to match the capacitance C_L of the line to the Blumlein value C_{B2}. Then, from equation (44), the expected magnitude of prepulse was $V = V_o/2$. The measurements showed this to be the case.

Since one of the problems brought about by the prepulse is the closing of spark gaps at the output (e.g. the gaps of the Travatron structure), a prepulse experiment was set up as shown in Figure 25. In this case, an atmospheric test gap was placed in series with the 50 ohm termination and means were provided for introducing a prepulse suppressor in the form of a shunt inductor.

The capacitative signal coupler had a time constant for too small to permit viewing of the prepulse. However, it provided a direct observation of the effect of the prepulse on the test gap as well as the effectiveness of the inductive shunt. Without the inductor the fast Blumlein pulse is equivalent to that obtained in the terminated load (Figure 24). This demonstrates that the prepulse pre-closed the test gap as expected. With the inductor installed, the reflection from the open switch is in evidence as illustrated by the brief reflection. It was also observed that the Blumlein output pulse was somewhat greater when the prepulse was suppressed in accord with the discussion presented above.

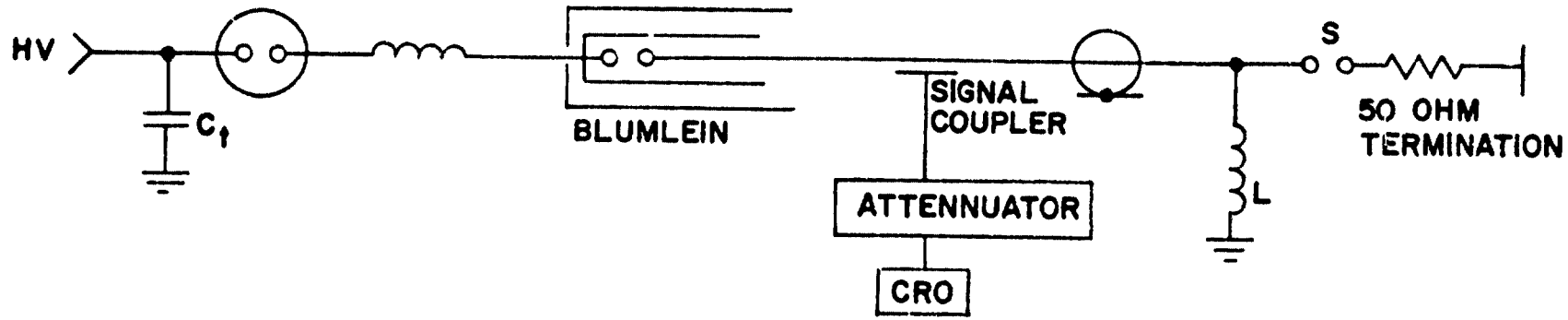

(a) TEST CONFIGURATION

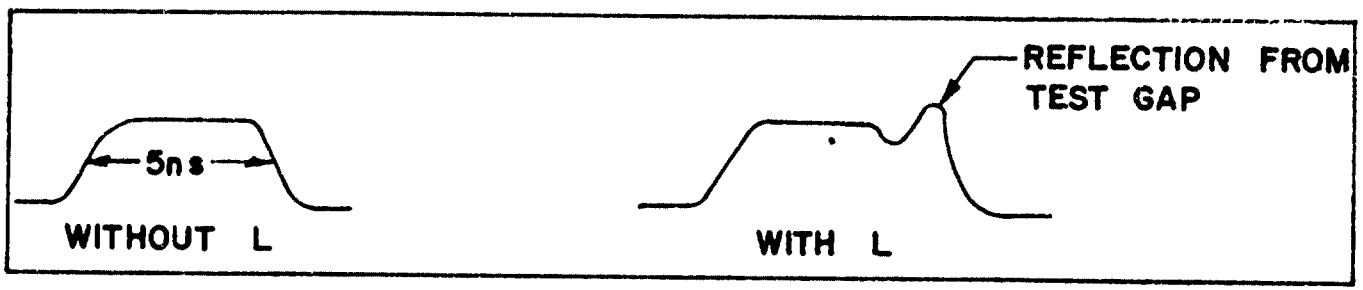

(b) TYPICAL WAVEFORMS

FIGURE 25

BLUMLEIN PREPULSE EXPERIMENT

SECTION IV

TRAVATRON BREADBOARD MODEL INVESTIGATION

1. DESIGN

The design approach for the Travatron breadboard model was derived from the considerations presented above in Section II-2. This led to a choice of the highest dielectric constant (K = 12) material available in a form useful for constructing the Travatron traveling wave structure. The success of the triaxial Blumlein as summarized in Section III-7 was also applied to the design of the breadboard and led to the integrated mechanical design shown in Figure 26. The optimum stress configuration as defined by equation (10) was first applied to the Blumlein. Using a dielectric with K = 12, the Blumlein was then constructed with two 8.5 ohm lines. The output impedance and, therefore, the impedance of the Travatron was then 17 ohms.

The physical dimensions of the Blumlein were chosen on the basis of stress levels and the desired output pulse length. The diameter of the inner conductor was 5/8" yielding a maximum stress from equation (8) in the range of 120 to 600 KV/mil for pulse charge potentials in the 20 KV to 100 KV range. The inside diameters of the intermediate and outer conductor then followed from the 8.5 ohm design to be 1.0" and 2.0" respectively. The length of the PFN portion of the Blumlein was 10" to produce a nominal 5 ns pulse output.

An "O" ring sealed, pressurized switch was designed as indicated in Figure 26 to provide variable self-breakdown up to the 100 KV level. The connection to the Travatron was made via a short section of high impedance line to form a low pass filter passing the video pulse but blocking the rf pulse generated in the Travatron. The prepulse was suppressed by means of an inductive path to ground as illustrated in the figure. Completing the signal separator portion of the Travatron a quarter-wave rf coupler was constructed to pass the generated rf pulse but to block the input video pulse from the output. Except for the use of a prepulse suppressor this video/rf

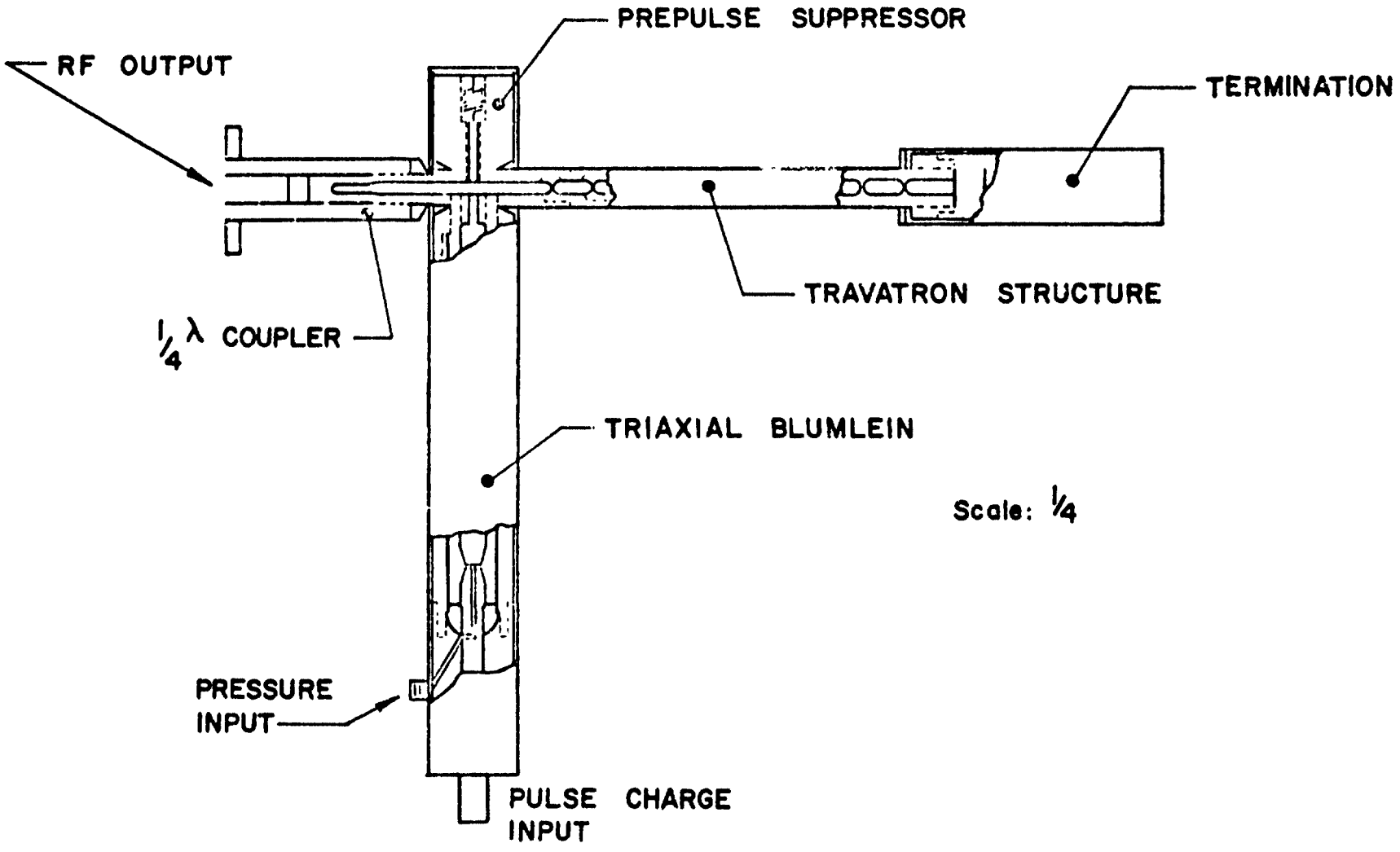

FIGURE 26

TRAVATRON BREADBOARD MECHANICAL DESIGN

pulse separation techniuqe is similar to that used in previous Travatrons such as described in Reference 2. The major difference from prior experience in the design illustrated in Figure 26 is the presence of the prepulse suppressor. Because of its complicating effect on the propagation path at this point, it was necessary in this case to adjust the suppressor inductance empirically using a cw source replacing the Travatron while determining the placement and value of the inductor.

The Travatron was designed to produce a 10-cycle waveform at a nominal output frequency of 1.3 GHz. The required nine segment traveling wave structure was composed of individual sections containing a center conductor segment and its associated dielectric. The 17 ohm structure was obtained with a Hi-K dielectric (K = 12), a one-inch ID outer conductor and a 3/8" diameter center conductor. The length of each segment was one inch to provide the correct propagation delay for the mixed propagation condition for the TEM wave in K = 12 material as well as in the gas space surrounding each spark switch. In assembly, the dielectric pieces were overlapped to maximize the creepage paths thus preventing high voltage surface breakdown. Gap spacings were variable by adjusting the individual center conductor locations with respect to the dielectric in a prescribed fashion. Such adjustment permitted gap settings over a range of 10 to 60 mils. The overall length of the traveling wave structure was approximately 10".

The termination shown in Figure 26 was designed to handle peak traveling wave potentials to 100 KV while dissipating up to 100 watts of average power. To accommodate these design requirements a heavy duty 17 ohm resistor was made up of a number of carbon resistors in a series/parallel stack. The assembly was subsequently potted in a high temperature/high conductivity epoxy.

Figure 27 is a photograph of the assembled breadboard as operated in the bench tests. The various elements of the system can be identified by reference to Figure 26. A signal coupler for viewing the output is seen at the output of the device.

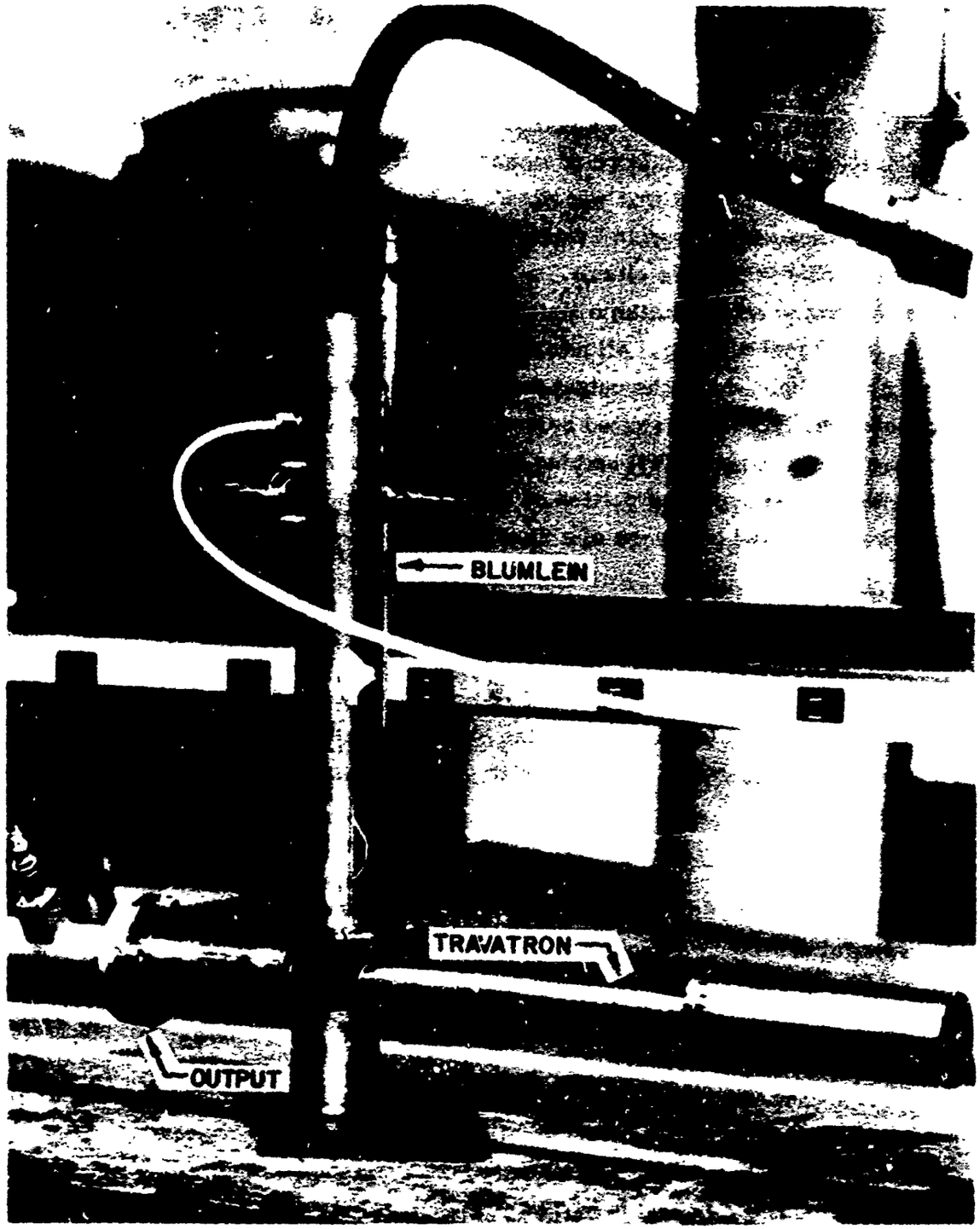

FIGURE 27

TRAVATRON BREADBOARD

2. TEST SET-UP

The overall test arrangement used in breadboard bench tests is illustrated in Figure 28. The system consisted of the Blumlein/Travatron breadboard just described in addition to means for energizing the Blumlein and for measurement of the output waveform. Pulse charging was accomplished by the technique discussed in Section III using a high voltage pulse transformer and charge transfer circuit. A specially designed 17 ohm load line was constructed with a suitable matched load and a wideband capacity divider for signal viewing. All measurements were made directly by observing the amplitude of the output pulse waveform on a traveling wave oscilloscope. For reasons cited below, additional tests were performed with the 17 ohm coaxial PFN serving as the input device. For these latter tests, the signal separator portion of the system was eliminated and the rf pulse was observed by means of a signal coupler placed in the input line.

3. FINDINGS

The findings achieved in operating the breadboard model fall into three general categories including: (a) voltage handling capability of the Blumlein and Travatron, (b) behavior of the Blumlein/Travatron special interface (prepulse suppressor) and (c) the ability of the Travatron design to produce high peak power.

As indicated in the above, the Hi-K material was used extensively in construction of both Blumlein and Travatron structures. In the Blumlein, the the material presented a number of difficulties associated with electromechanical properties. In the forms required for the Blumlein the material was easily damaged by mechanical and thermal stresses developed in both machining and assembly. Its voltage handling capability was affected by even minor damage of this type. Moreover, the material was noted to possess minor flaws (e.g. voids) greatly reducing the breakdown fields which could be sustained. Thus, its working dielectric strength was apparently greatly different from the intrinsic breakdown strength of the material. In the Blumlein design the maximum stress was, of course,

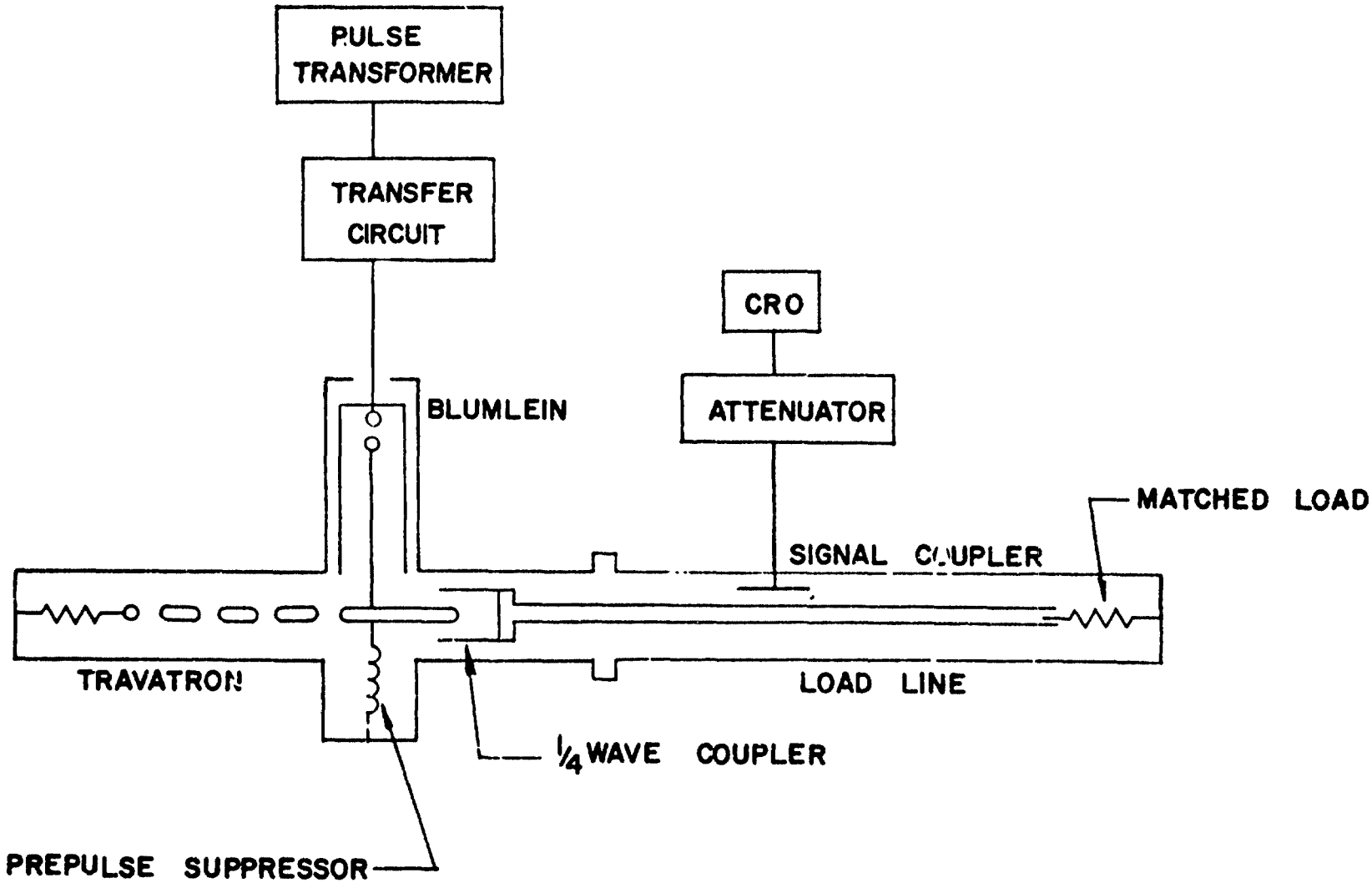

FIGURE 28

TRAVATRON BREADBOARD SYSTEM

considerably above the manufacturers rating.

By contrast, voltage handling in the structures following the output of the Blumlein presented no difficulty whatsoever. No voltage failures were encountered in the signal separator region nor in the Travatron structure. This marked difference in the voltage stress capability of the Hi-K material is probably due to the time scales of the voltage pulses applied in these portions of the system. In operation, the Blumlein sustains stresses due to the input charge potential for times on the order of 10^{-7} sec, while in the remainder of the system, the applied voltage is present for at most a few nanoseconds.

The basic function of the Blumlein, signal separator and prepulse suppressor was nominal except for the occasional voltage handling problem just cited. At one point in the investigation, the prepulse suppression technique was suspected of interfering with Travatron performance, but this was later shown not to be the case during the aforementioned testing with the coaxial PFN in which Travatron performance was similar for a similar input pulse.

The output of the breadboard Travatron was expected to lie in the range of 5 - 100 MW for input traveling wave heights in the 20 to 100 KV range based on the analysis summarized in Section II-1, 2. This result did not materialize, however, and a maximum power level of 10.8 MW was observed at an input pulse height of 45 KV. The experimental effort using the breadboard was focussed largely on determining the underlying cause for this apparent peak power limitation. Various causes associated with the pre-pulse suppression technique, adjustments of the Travatron structure (e.g. gap spacings) and corona discharge at the interface of conductors and Hi-K material were explored and eliminated. The analysis presented in Section II-3 reveals that the cause lies in the impedance value chosen for the basic design. At 1.3 GHz, the analysis predicts a maximum attainable power $P_{max} \triangleq 0.8Z = 13.6$ MW for the 17 ohm device. Considering the various approximations used in the analysis this is in good agreement with the experimentally observed limit for this Travatron. According to the same

analysis, to achieve 100 MW operation would require a 125 ohm design.

SECTION V

CONCLUSIONS AND RECOMMENDATIONS

This investigation has encompassed many of the key elements associated with upgrading the design and implementation of the high power Travatron transmitter. Analysis has been conducted which quantitatively defines the design of the Travatron structure while also defining upper bounds on peak power to be expected from single devices operating at various frequencies. New techniques have been explored for efficient, compact hardware to generate input voltage pulses needed to activate the Travatron. The specific accomplishments and findings of the investigation may be highlighted as follows:

(1) Design analysis has been performed which optimizes the peak power-to-weight ratio of the Travatron. Order of magnitude improvement over previous designs is now seen possible.

(2) In conjunction with the above optimization the use of high dielectric constant insulating materials has been explored as a means for realization of these gains and guidelines for employing such materials have been established.

(3) The limits of peak power capabilities for simple Travatron structures has been determined analytically as a function of device impedance and operating frequency. Based on experience with one device the limit dependence, and therefore the analytical model used, is supported.

(4) The design analysis results in a need for higher rather than lower impedance devices for maximum power capability at a given frequency. According to the analysis, the peak power limit is directly proportional to the impedance and obeys an approximate negative three-halves power frequency dependence. At 1 GHz, 100 MW peak power can be expected from 100 ohm devices employing a singly switched Travatron structure.

(5) The systematics of developing suitable high voltage input pulses for the Travatron have been investigated through several candidate schemes making the transition from prime power through transient voltage step-up schemes to the formation of the input pulse.

(6) The triaxial Blumlein has been investigated experimentally. Except for the minor problems associated with suppression of the pre-pulse, the Blumlein has been demonstrated as a useful PFN device for developing high voltage, nanosecond input pulses for the Travatron. The utility of the device is underscored by needs for high pulse potentials associated with high impedance Travatrons operating near the design limits.

(7) A preliminary model of a piezoelectric pulse generator has been successfully tested and, in conjunction with this generator, a concept employing pressurized gas for prime energy storage has been employed. The development of a 100 KV pulser producing several joules of pulse energy is a straightforward extension of the model constructed in this program.

(8) A spiral line pulse generator has been constructed and tested as a candidate device for interfacing relatively low prime power voltages to those suitable for multi-megawatt Travatrons.

Further development work should seek to extend the Travatron state-of-the-art along the guidelines which may be derived from the analysis and experimentation of this program. In the quest for greater peak power capability, the findings regarding peak power limits should be refined and tested. Analytically an attempt should be made to include factors such as the rise time of the incident pulse on the Travatron switch and the effects of electrode material and gaseous environment on field emission. Experimentally, the frequency and impedance dependence of peak power limits should be investigated in a systematic manner.

The directly recommended approach for achieving maximum peak power involves high impedance design which, in practice, is constrained to impedance levels not much greater than 100 ohms. An alternate approach suggested by the analysis of this program is to parallel the switch structure within the Travatron if not to parallel complete Travatron devices. The required synchronization method is available by optical methods.

An additional avenue for future development involves the intriguing possibility of modifying the basic function of the Travatron switch from one governed by statistical lag to one controlled by the formative component of lag. This approach might be tenable by employing high pressure, closely spaced spark switches.

Among the various pulse power sources considered in this program, the piezoelectric generator is particularly interesting in its direct conversion of mechanical to electrical energy at high potential. The peizoelectric generator for generation of energetic, sub-microsecond pulses has been demonstrated in this program and could be extended rapidly toward more ambitious output levels. It is recommended that additional work be conducted in this area.

REFERENCES

1. J. M. Proud, "Radio Frequency Generators", U.S. Patent No. 3,484,619.

2. J. M. Proud, H. Huber, W. Hirtle, "A Megawatt L-Band Travatron for Direct Generation of Nanosecond Pulses", RADC-TR-68-254.

3. J. M. Proud and H. Huber, "Picosecond Rise Time Switch Study", RADC-TR-67-400 (1967).

4. P. Felsenthal and J. M. Proud, Phys. Rev. 139, A1796 (1965).

5. G. N. Glascoe and J. V. Lebacqy, Radiation Sub Series, Vol. 5, McGraw-Hill (1948).

6. J. J. Moriarty, H. I. Milde and J. E. Hipple, "Megavolt Modulator Study", RADC-TR-70-107 (1970).

7. J. P. Arndt, "Piezoelectric High Voltage Generators", Clevite Report No. TP-219.

8. R. A. Fitch and V. T. S. Howell, Proc. IEE, 111, No. 4, 849 (1965).

9. D. J. Brosan, "An Electrical Machine for Use in Extra-Terrestrial Environment", Astronautica Acta, p. 270, November 1955.

10. M. Alperin and G. P. Sutton, Advanced Propulsion Systems (Symposium), pp. 161, Pergamon Press, New York (1959).

*U.S. GOVERNMENT PRINTING OFFICE: 1973-713-122/45